USING IMPROVED BACKGROUND ERROR COVARIANCES FROM AN ENSEMBLE KALMAN FILTER FOR ADAPTIVE OBSERVATIONS

Thomas M. Hamill

NOAA-CIRES Climate Diagnostics Center

Boulder, Colorado

Chris Snyder

National Center for Atmospheric Research,[*]

Boulder, Colorado

submitted to *Monthly Weather Review*

24 April 2001

[*] The National Center for Atmospheric Research is sponsored by the National Science Foundation

Corresponding author address: Dr. Thomas M. Hamill, NOAA-CIRES Climate Diagnostics Center, R/CDC 1, 325 Broadway, Boulder, CO 80303-3328. hamill@cdc.noaa.gov ; (303) 497-3060 ; telefax (303) 497-7013

ABSTRACT

A method for selecting targeted observation locations is demonstrated. This method is based on optimal estimation (Kalman filter) theory; it determines the observation location which will maximize the expected improvement, which can be measured in terms of the expected reduction in analysis or forecast variance. This technique requires an accurate model for background error statistics that will vary both in space and in time. Here, these covariances are generated using an ensemble Kalman filter techniques.

The technique is demonstrated using a quasigeostrophic channel model under perfect-model assumptions. The algorithm is applied here to find the supplemental rawinsonde site to add to a regular network of rawinsondes that will reduce analysis errors the most. The observation network is configured in this experiment so there is a void in the western third of the domain. Ensembles from three data assimilation schemes are tested as input to the target selection procedure, two variants of the standard ensemble Kalman filter and a third perturbed observation (3D-Var) ensemble. The technique is shown to find large differences in the expected variance reduction depending on the observation location, the flow of the day, and the ensemble used in the targeting algorithm. The two variants of the ensemble Kalman filter defined consistently similar targets to each other, and assimilation of the targeted observation typically reduced analysis errors significantly. The perturbed observation ensemble picked very different observation locations and the analyses were the analyses improved as much.

The amount of improvement from assimilating a supplemental targeted observation instead of a fixed observation in the middle of the void depended on whether the observation was assimilated intermittently or during every analysis cycle. For intermittent assimilation, the targeted observation provided a dramatic improvement relative to the supplemental fixed observation. When continuously assimilated, the improvement was smaller.

For the intermittent assimilation of a targeted observation, targeting based on the maximum spread in background forecasts in the ensemble Kalman filter provided similar target locations and similar analysis improvements to those generated with the full algorithm. The continuous assimilation of targets based on the spread algorithm was no better than when observations from a fixed target in the middle of the void were assimilated.

1. INTRODUCTION

It has long been recognized that the quality of a numerical weather forecast is related to the quality of its initial condition (the "analysis"). If the analysis has large errors, or if it has moderate errors in regions where forecast errors grow quickly, then the resulting numerical forecast may be poor.

Let us assume that in addition to a routine network of observations, additional observations could be collected sporadically for a moderate cost. These observations, which might come from dropsondes, pilotless drones, or driftsondes, would be taken at a location(s) chosen to maximize the expected improvement in some aspect of the ensuing analysis or the subsequent forecasts. This general problem is known as *targeting*, or *adaptive observations* (Emanuel et al. 1995, Snyder 1996, Lorenz and Emanuel 1998).

Most existing methods for targeted observations are at least in part heuristic, as their development has been driven by practial opportunities in field experiments such as FASTEX (Snyder 1996, Joly et al. 1997, Emanuel and Langland 1998), NORPEX (Langland et al. 1999a) and the Winter Storms Reconaissance Program (Szunyogh et al. 2000). These methods include the singular vector technique (Palmer et al. 1998, Buizza and Montani 1999, Bergot et al. 1999, Gelaro et al. 1999, 2000, Bergot 2001); a quasi-linear inverse approach (Pu et al. 1997, 1998, Pu and Kalnay 1999); gradient and sensitivity approaches (Bergot et al. 1999, Langland et al. 1999b, Baker and Daley 2000), ensemble spread techniques (Lorenz and Emanuel 1998, Morss 1998, Morss et al. 2001), the ensemble transform technique (Bishop and Toth 1999, Szunyogh et al. 1999), and the ensemble transform Kalman filter (Bishop et al. 2001, Majumdar et al. 2001).

In this paper we step back to consider the targeting problem on a somewhat more theoretical level. Choosing observation locations requires that we predict the influence of a given observation on the uncertainty of the analysis or the subsequent forecast. That influence is determined not only by the form and accuracy of the observation and how errors will grow during the subsequent forecast (if we are interested in forecasts), but also by the prior or background uncertainty given all other available information, such as other observations and previous forecasts. Berliner

et al. (1999) provide the analytical tools for understanding how analysis and forecast uncertainty are related to observation and background uncertainty. Their framework, which is reviewed in section 2, is an application of ideas of statistical design and estimation theory to targeted observations (see their Section 2, Appendix A, and Cohn 1997). The choices of observation locations derived through this framework are optimal in the case that the required probability distributions are normal and forecast-error evolution is linear. This framework differs from many of the existing approaches that do not consider the effects of background uncertainty, such as the singular vector technique or sensitivity techniques (as implemented in practice, though not in principle; see Ehrendorfer and Tribbia 1997, Barkmeijer et al. 1998, Palmer et al. 1998). As a consequence, when using these schemes, the same target location is selected regardless of how large or small the background error is in a given location, and regardless of how accurate or inaccurate the observation (Baker and Daley 1999).

The data assimilation scheme is an additional factor that determines the influence of an observation on the background uncertainty. Results from field experiments show that adding observations to operational analysis/forecast systems can degrade subseqent forecasts, and this has often been blamed on inadequacies of the operational assimilation schemes. (Bergot 2001) found that supplemental observations provided a more consistently positive impact when they were assimilated with a 4-dimensional variational analysis (4D-Var; Le Dimet and Talagrand 1986, Rabier et al 1998) rather than a 3-dimensional variational analysis (3D-Var; Lorenc 1986, Parrish and Derber 1992). Note, however, that such degradations are inherent in statistical assimilation schemes; see Morss and Emanuel (2001). We show here in section 2 that, given a good estimate of the background uncertainty, the effects of sub-optimal assimilation schemes can be incorporated when predicting the influence of an observation.

Our primary intent in this paper is to demonstrate a relatively simple, objective, and computationally efficient algorithm for target selection based on and consistent with Berliner et al. (1999). To wit, we shall use an ensemble of forecasts coupled to three different data assimilation schemes, including two variants of the ensemble Kalman filter ("EnKF;" Evensen 1994;

Evensen and van Leeuwen 1996; Houtekamer and Mitchell 1998, 2001; van Leeuwen 1999, Keppenne 2000; Mitchell and Houtekamer 2000; Hamill and Snyder 2000, Hamill et al. 2001, Anderson 2001, Whitaker and Hamill 2001). Under the assumptions of a perfect model, an infinite ensemble, normality of observation and background errors, and linearity of error growth, the ensemble Kalman filter provides the minimum variance estimate of an updated analysis state and a correct model of the analysis covariances given all prior and currently available observations (Burgers et al. 1998). We demonstrate that a target selection algorithm with an approximate model of background error covariances provided by a large ensemble is able to identify target locations where analysis improvement is likely to be the largest. Its straightforward and computationally efficient design permits it to estimate the magnitude of the variance reduction at each of a multitude of possible target locations; the targeting algorithm then selects the location where this variance is reduced by a maximum expected amount. We will also develop but not test a targeting algorithm that can find the observation locations which maximize the expected reduction in forecast error.

Others investigations of targeting have used ensemble techniques to estimate background uncertainty (Lorenz and Emanuel 1998, Bishop and Toth 1999, Morss et al. 2000, Hansen and Smith 2000). Only Bishop et al. (2001), however, have used that estimate to calculate explicity the influence of an given observation. Our technique is mathematically equivalent to theirs (and both are approximations to the results of Berliner et al. (1999)); we present here a computationally more efficient approach to the calculations valid for simple observation types and demonstrate that estimates of background uncertainty from the EnKF allow accurate predictions of the influence of further observations.

In part to limit the scope of this paper, we focus on choosing additional observations to minimize expected analysis errors. The algorithm we develop, however, has a straightforward extension to the case of minimizing expected forecast errors, as described in section 3d. Minimizing expected analysis errors is also of interest in its own right, as it is the natural approach if one desires to optimize forecast quality simultaneously at multiple lead times or from multiple ini-

tialization times (Berliner et al. 1999). Minimizing expected analysis errors also avoids potential complications arising from the nonlinearity of forecast dynamics, and the associated non-Gaussianity of forecast errors (Hansen and Smith 2000); the algorithm we derive will be useful only when forecast errors are not too far from Gaussian.

2. DESIGN OF THE EXPERIMENT

The rest of the paper will use a quasigeostrophic (QG) channel model as vehicle for testing algorithms for targeting. The target selection scheme will be tested using ensembles coupled with three different data assimilation schemes, two variants of an ensemble Kalman filter and a "perturbed observation" (Houtekamer and Derome 1995, Hamill et al. 2000) 3D-Var scheme.

For these experiments we assume the forecast model is perfect. A long reference integration of the QG model provides the true state; the assimilation and forecast experiments then use that same model together with imperfect observations of the true state.

Errors will be measured in a total energy norm. Let f denote the Coriolis parameter (here, $10^{-4}s^{-1}$); m is the dimension of the model state vector; N is the Brunt-Väisälä frequency (here, $1.13 \times 10^{-2}s^{-1}$), and Φ' is a geopotential perturbation. Then the energy norm is denoted as

$$\| \cdot \|_{energy} = f^{-1}m^{-1/2} \times \left\{ \sum_{j=1}^{m} \left[\left(\frac{\partial \Phi'}{\partial x} \right)_j^2 + \left(\frac{\partial \Phi'}{\partial y} \right)_j^2 + \frac{f^2}{N^2} \left(\frac{\partial \Phi'}{\partial z} \right)_j^2 \right] \right\}^{1/2}. \quad (1)$$

a. Model and Observations

The QG model is documented in Snyder et al. (2001) and was used in Hamill and Snyder (2000) and Hamill et al. (2000). It is a mid-latitude, beta-plane, grid-point channel model that is periodic in x (east-west), has impermeable walls on the north-south boundaries, and rigid lids at the top and bottom. There is no terrain, nor are there surface variations such as land and water. Pseudo-potential vorticity (PV) is conserved except for Ekman pumping at the surface, ∇^4 horizontal diffusion, and forcing by relaxation to a zonal mean state. The domain is 16000 $\times$ 8000 $\times$ 9 km; there are 129 grid points east-west, 65 north-south, and 8 model forecast levels, with additional staggered top and bottom levels at which potential temperature θ is specified. Forecast model parameters are set as in Hamill et al. (2000).

A single fixed observational network is tested here (Fig. 1), with a data void in the western third of the domain. All observations are presumed to be rawinsonde soundings, with u- and v-wind components and θ observed at each of the 8 model levels. Observation errors (Table 1) are assumed to be normal and uncorrelated between vertical levels and uncorrelated in time. The same observation error variances are used in the data assimilation and in the generation of synthetic "control" observations. These observations and new analyses are generated every 12 h, followed by a 12-h forecast with the QG model that produces the background state at the next analysis time.

b. Data assimilation schemes.

The targeting algorithm to be described in the section 3 requires an ensemble whose sample covariance matrix approximates that of the background errors (prior to the assimilation of the additional observations). That ensemble will depend on the specific data assimilation scheme used to assimilate previous observations.

We will use three assimilation schemes, a 3D-Var algorithm and two variants of the EnKF. All are described in detail in the Appendix, and parameter settings in Table 2. The two versions of the EnKF differ in the way that background error covariances are approximated given an ensemble of background states. In the first, the deviation of each member from the ensemble mean is "inflated" (that is, multiplied by a scalar constant greater than 1) before their use in the EnKF. In the second, the assimilation is based on a "hybrid" covariance model in which the background error covariance matrix is approximated as a weighted sum of the sample covariance from the ensemble and a stationary covariance matrix (specifically, that used in the 3D-Var scheme). Both versions of the EnKF use covariance localization as discussed in the Appendix.

The required ensemble is generated in the same manner for each of these assimilation schemes. Suppose that we have an ensemble of prior forecasts. Then, given new observations, each member of this ensemble is updated separately with those observations perturbed by an independent realization from the observation-error distribution; this we term a "perturbed observation" scheme. The resulting ensemble of analysis can then be used to produce an ensemble of short-range fore-

casts valid at the next observation time. Previous work has shown that in a perfect-model context, such ensembles have desirable sampling characteristics for when used either with a 3D-Var assimilation (Hamill et al. 2000) or in the context of the EnKF (Houtekamer and Mitchell 1998, 2001; Hamill and Snyder 2000). Again, further details of the implementation appear in the Appendix. For ensemble data assimilation schemes that do not involve perturbing the observations, see Lermusiaux and Robinson (1999), Anderson (2001), and Whitaker and Hamill (2001).

3. METHODOLOGY FOR CHOOSING TARGET LOCATIONS

The methodology we implement for the selection of a target location follows closely from the theory of Berliner et al. (1999). Although more efficient computationally, this methodology is mathematically identical to that of Bishop et al. (2001) in its use of an ensemble to estimate the required background error covariance matrix. Our emphasis here is to demonstrate that this rigorous approach to adaptive observations is feasible and effective, in that it can accurately predict the effect of observations on analysis uncertainty using a relatively small ensemble. In addition, this methodology is able to predict the impact of additional observations even when those observations are assimilated with a sub-optimal assimilation scheme. Notation generally follows the suggestions of Ide et al. (1997).

a. Equations to predict analysis-error variance

First, consider the analysis calculation, written in the general form

$$\mathbf{x}^{\mathrm{a}} = \mathbf{x}^{\mathrm{b}} + \hat{\mathbf{K}}\left(\mathbf{y}^{\mathrm{o}} - \mathbf{H}\mathbf{x}^{\mathrm{b}}\right) = \left(\mathbf{I} - \hat{\mathbf{K}}\mathbf{H}\right)\mathbf{x}^{\mathrm{b}} + \hat{\mathbf{K}}\mathbf{y}^{\mathrm{o}} \tag{2}$$

where $\mathbf{x}^{\mathrm{a}}$ is the m-dimensional analyzed state vector $\mathbf{y}^{\mathrm{o}}$ is a p-dimensional vector of observations, $\hat{\mathbf{K}}$ is an approximate gain matrix defined below, and $\mathbf{x}^{\mathrm{b}}$ is the background state, which is typically a forecast from the previous analysis but more generally is our best estimate of the state prior to assimilating the observations $\mathbf{y}^{\mathrm{o}}$. The linear operator $\mathbf{H}$ relates the true state $\mathbf{x}^{\mathrm{t}}$ to the observations through

$$\mathbf{y}^{\mathrm{o}} = \mathbf{H}\mathbf{x}^{\mathrm{t}} + \epsilon, \quad \epsilon \sim N(0, \mathbf{R}), \tag{3}$$

In reality, the relation between the model state and the observations is often nonlinear, and most existing assimilation schemes satisfy (2) and (3) only approximately.

The gain matrix $\hat{\mathbf{K}}$ is specific to the assimilation scheme. In all the schemes considered here, $\hat{\mathbf{K}}$ has the form

$$\hat{\mathbf{K}} = \hat{\mathbf{P}}^{\mathrm{b}}\mathbf{H}^{\mathrm{T}}\left(\mathbf{H}\hat{\mathbf{P}}^{\mathrm{b}}\mathbf{H}^{\mathrm{T}} + \mathbf{R}\right)^{-1}, \tag{4}$$

where $\hat{\mathbf{P}}^{\mathrm{b}}$ is a model or approximation of the actual backround error covariance matrix,

$$\mathbf{P}^{\mathrm{b}} = \left\langle (\mathbf{x}^{\mathrm{t}} - \mathbf{x}^{\mathrm{b}})(\mathbf{x}^{\mathrm{t}} - \mathbf{x}^{\mathrm{b}})^{\mathrm{T}} \right\rangle, \tag{5}$$

where $\langle \cdot \rangle$ denotes the expected value. For example, many 3D-Var systems use $\hat{\mathbf{P}}^{\mathrm{b}} = \mathbf{B}$, where $\mathbf{B}$ is a stationary, isotropic covariance matrix, while the EnKF bases $\hat{\mathbf{P}}^{\mathrm{b}}$ on the sample covariance of an ensemble of background states.

Next, we derive a general expression for the analysis error covariance,

$$\mathbf{P}^{\mathrm{a}} = \left\langle (\mathbf{x}^{\mathrm{t}} - \mathbf{x}^{\mathrm{a}})(\mathbf{x}^{\mathrm{t}} - \mathbf{x}^{\mathrm{a}})^{\mathrm{T}} \right\rangle. \tag{6}$$

Subtracting both sides of (2) from $\mathbf{x}^{\mathrm{t}}$ gives

$$\mathbf{x}^{\mathrm{t}} - \mathbf{x}^{\mathrm{a}} = \left(\mathbf{I} - \hat{\mathbf{K}}\mathbf{H}\right)(\mathbf{x}^{\mathrm{t}} - \mathbf{x}^{\mathrm{b}}) + \hat{\mathbf{K}}\epsilon. \tag{7}$$

Substituting this result into (6) and assuming that the observation and background errors are uncorrelated, i.e., $\left\langle \epsilon \left(\mathbf{x}^{\mathrm{t}} - \mathbf{x}^{\mathrm{b}}\right)^{\mathrm{T}} \right\rangle = 0$, we obtain

$$\begin{aligned} \mathbf{P}^{\mathrm{a}} &= \left(\mathbf{I} - \hat{\mathbf{K}}\mathbf{H}\right)\mathbf{P}^{\mathrm{b}}\left(\mathbf{I} - \hat{\mathbf{K}}\mathbf{H}\right)^{\mathrm{T}} + \hat{\mathbf{K}}\mathbf{R}\hat{\mathbf{K}}^{\mathrm{T}} \\ &= \mathbf{P}^{\mathrm{b}} - \hat{\mathbf{K}}\mathbf{H}\mathbf{P}^{\mathrm{b}} - \left(\hat{\mathbf{K}}\mathbf{H}\mathbf{P}^{\mathrm{b}}\right)^{\mathrm{T}} + \hat{\mathbf{K}}\left(\mathbf{H}\mathbf{P}^{\mathrm{b}}\mathbf{H}^{\mathrm{T}} + \mathbf{R}\right)\hat{\mathbf{K}}^{\mathrm{T}} \end{aligned} \tag{8}$$

If the assimilation scheme uses the correct background error covariance matrix ($\hat{\mathbf{P}}^{\mathrm{b}} = \mathbf{P}^{\mathrm{b}}$), then $\hat{\mathbf{K}}$ becomes the Kalman gain matrix, $\mathbf{K} = \mathbf{P}^{\mathrm{b}}\mathbf{H}^{\mathrm{T}}(\mathbf{H}\mathbf{P}^{\mathrm{b}}\mathbf{H}^{\mathrm{T}} + \mathbf{R})^{-1}$, and

$$\mathbf{P}^{\mathrm{a}} = \left(\mathbf{I} - \mathbf{K}\mathbf{H}\right)\mathbf{P}^{\mathrm{b}} = \mathbf{P}^{\mathrm{b}} - \mathbf{P}^{\mathrm{b}}\mathbf{H}^{\mathrm{T}}\left(\mathbf{H}\mathbf{P}^{\mathrm{b}}\mathbf{H}^{\mathrm{T}} + \mathbf{R}\right)^{-1}\mathbf{H}\mathbf{P}^{\mathrm{b}}, \tag{9}$$

which is the familiar updating of covariances in the Kalman filter.

Equations (8) and (9) thus provide us with a framework for estimating analysis error covariances for a given **H** in the case of imperfect and perfect background error statistics, respectively. These equations express how assimilation of new observations changes the uncertainty of the analysis relative to that of the background. This change depends on the form and location of the observations through **H**, the data assimilation scheme through $\hat{\mathbf{K}}$, and the background uncertainty through $\mathbf{P}^{\mathrm{b}}$. Conversely, given **H**, $\hat{\mathbf{K}}$, and $\mathbf{P}^{\mathrm{b}}$ (or at least a good estimate of the latter), the change in the analysis uncertainty is determined. In particular, that change does not depend on the actual observations $\mathbf{y}^{\mathrm{o}}$ and one can predict the effects of additional observations prior to the measurements themselves (Berliner et al. 1999).

We emphasize that (8) accounts naturally for the assimilation scheme and, moreover, that the influence of the assimilation scheme on the analysis uncertainty can not be fully quantified without knowledge of the true $\mathbf{P}^{\mathrm{b}}$. In addition, note that while the derivation of (8) and (9) does not make assumptions about the form of the underlying probability distributions for the forecast and analysis, those equations will be useful only when the covariance matrices $\mathbf{P}^{\mathrm{a}}$ and $\mathbf{P}^{\mathrm{b}}$ are useful summaries of uncertainty, that is, when those distributions are not too far from Gaussian. The usefulness of (8) is also limited to those assimilation schemes in which the update is approximately linear as assumed in (2).

b. Targeting to reduce analysis error variance

Now suppose we want to choose the location of a single observation to minimize the expected analysis error variance.[1] Formally, this amounts to maximizing $tr(\mathbf{P}^{\mathrm{b}} - \mathbf{P}^{\mathrm{a}})$ over a set of observation operators **H** consisting of all possible locations for the observation. Assuming hereafter that an ensemble is available that provides a reasonable and computationally tractable estimate of $\mathbf{P}^{\mathrm{b}}$, then (8) or (9) allow us to determine the best **H** by evaluating $tr(\mathbf{P}^{\mathrm{b}} - \mathbf{P}^{\mathrm{a}})$ for each **H**. Typically, this additional observation will supplement an existing network of routine observa-

[1] This minimization can be carried out for measures of uncertainty other than total variance. A variety of choices are discussed in Berliner et al. (1999).

tions. The background or prior estimate to which $\mathbf{P}^b$ pertains is then the analysis with all routine observations.

For each potential observation location, there is an associated $\mathbf{H}$; however, it may be economically feasible to target more than one location at a time. With two target locations, one would potentially have to evaluate all the combinations of locations to find the two that would reduce variance the most. Instead, we will make the simplifying assumption that the correct combination of target locations can be determined with a serial, or "greedy" algorithm (Lu et al. 2000, Bishop et al. 2001). This serial approach is applicable when successive observations have independent errors.

Specifically, to determine a sequence of multiple target locations, the following steps are repeated: first, $tr(\mathbf{P}^b - \mathbf{P}^a)$ is computed for each candidate observation location (each $\mathbf{H}$). The location with the maximum trace is then selected, and an updated ensemble is generated whose sample covariance approximates $\mathbf{P}^a$ implied by assimilating an observation at that location (note that real observations need not be assimilated at this point; the important detail is that the ensemble can be updated with some synthetic set of observations, since (8) and (9) depend only on the observation error covariance $\mathbf{R}$ and not on the actual observations.) The targeting algorithm is then applied again using the updated ensemble of analyses as background forecasts to select the next target location.

If the observations will be assimilated using a relatively simple model of background error covariances, perhaps as are used in 3D-Var, then (8) should be used instead of (9) and prediction of the variance reduction in (8) requires an ensemble (such as the perturbed-observation ensemble discussed in the Appendix) that reflects uncertainty in the background using a given assimilation scheme. Of course, if the ensemble estimate of $\mathbf{P}^b$ is good enough for this purpose, it would also be natural to include it in the assimilation scheme and (8) would not be required.

b. Making the targeting algorithm computationally efficient

The algorithm just outlined involves evaluating the influence of an observation on the analysis error over many different observation locations. In this section, we outline a relatively inex-

pensive technique for computing the expected reduction in analysis variance for a given observation.

The technique begins from an ensemble of background states, written as $\{\mathbf{x}_i^{\mathrm{b}},\ i = 1, \ldots, n\}$ where subscripts denote ensemble members. The ensembles considered here all approximate random samples from the the conditional distribution of $\mathbf{x}^{\mathrm{t}}$ given other information. The background state $\mathbf{x}^{\mathrm{b}}$ is thus replaced by the ensemble mean, $\vec{\mathbf{x}}^{\mathrm{b}} = (1/n)\sum_{i=1}^{N} \mathbf{x}_i^{\mathrm{b}}$, and $\mathbf{P}^{\mathrm{b}}$ is estimated in (8) and (9) by

$$\hat{\mathbf{P}}^{\mathrm{b}} = \frac{1}{n-1}\sum_{i=1}^{n}(\mathbf{x}_i^{\mathrm{b}} - \vec{\mathbf{x}}^{\mathrm{b}})(\mathbf{x}_i^{\mathrm{b}} - \vec{\mathbf{x}}^{\mathrm{b}})^{\mathrm{T}} = \mathbf{X}^{\mathrm{b}}\mathbf{X}^{\mathrm{b}^{\mathrm{T}}}, \tag{10}$$

where $\mathbf{X}^{\mathrm{b}}$ is the matrix whose ith column is $(n-1)^{-1/2}(\mathbf{x}_i^{\mathrm{b}} - \vec{\mathbf{x}}^{\mathrm{b}})$. For the remainder of this section, we will simply replace $\mathbf{P}^{\mathrm{b}}$ by $\hat{\mathbf{P}}^{\mathrm{b}}$ in (9), with the assumption that $\hat{\mathbf{P}}^{\mathrm{b}}$ approximates $\mathbf{P}^{\mathrm{b}}$ with sufficient accuracy. Our subsequent results will demonstrate that this is so in a moderately complex, quasigeostrophic model.

If we are evaluating the reduction from assimilating a single radiosounding, the matrix $\left(\mathbf{H}\mathbf{P}^{\mathrm{b}}\mathbf{H}^{\mathrm{T}} + \mathbf{R}\right)$ is of full rank, relatively low order, symmetric, and positive definite. Hence it can be decomposed as $\mathbf{Q}\Lambda_o\mathbf{Q}^{\mathrm{T}}$, where $\mathbf{Q}$ is an orthogonal matrix whose columns are the normalized eigenvectors and and Λ_o a diagonal matrix of associated eigenvalues. Since $\mathbf{Q}^{-1} = \mathbf{Q}^{\mathrm{T}}$,

$$\left(\mathbf{H}\mathbf{P}^{\mathrm{b}}\mathbf{H}^{\mathrm{T}} + \mathbf{R}\right)^{-1} = \mathbf{Q}\Lambda_o^{-1}\mathbf{Q}^{\mathrm{T}} = \left(\mathbf{Q}{\Lambda_o}^{-1/2}\right)\left(\mathbf{Q}{\Lambda_o}^{-1/2}\right)^{\mathrm{T}}, \tag{11}$$

and hence, from (9),

$$\mathbf{P}^{\mathrm{b}} - \mathbf{P}^{\mathrm{a}} = \left(\mathbf{P}^{\mathrm{b}}\mathbf{H}^{\mathrm{T}}\mathbf{Q}\Lambda_o^{-1/2}\right)\left(\mathbf{P}^{\mathrm{b}}\mathbf{H}^{\mathrm{T}}\mathbf{Q}\Lambda_o^{-1/2}\right)^{\mathrm{T}} \tag{12}$$

However, in computing the term in parentheses on the right-hand side of (12), a matrix multiplication by $\mathbf{P}^{\mathrm{b}}$ is still necessary, and if $\mathbf{H}$ is sparse, this typically will be the most computationally intensive step.

In calculating the trace of (12), the product $\mathbf{P}^{\mathrm{b}}\mathbf{H}^{\mathrm{T}}$ is evaluated as $\mathbf{X}^{\mathrm{b}}(\mathbf{H}\mathbf{X}^{\mathrm{b}})^{\mathrm{T}}$ as in (A2) from Appendix 1. To render this more computationally efficient, we perform a singular-value decomposition on $\mathbf{X}^{\mathrm{b}}$, so that

$$\mathbf{X}^{\mathrm{b}} = \mathbf{U}\Sigma\mathbf{V}^{\mathrm{T}}, \tag{13}$$

where $\mathbf{U}$ is an $m \times (n-1)$ matrix with orthonormal columns, $\mathbf{\Sigma}$ is an $(n-1) \times (n-1)$ diagonal matrix of non-zero singular values, and $\mathbf{V}$ is an $(n-1) \times (n-1)$ orthogonal matrix. Similarly, $\mathbf{HX}^{\mathrm{b}} = \mathbf{HU\Sigma V}^{\mathrm{T}}$ so $(\mathbf{HX}^{\mathrm{b}})^{\mathrm{T}} = \mathbf{V}^{\mathrm{T}}\mathbf{\Sigma}^{\mathrm{T}}(\mathbf{HU})^{\mathrm{T}} = \mathbf{V}^{\mathrm{T}}\mathbf{\Sigma}(\mathbf{HU})^{\mathrm{T}}$ since $\mathbf{\Sigma}^{\mathrm{T}} = \mathbf{\Sigma}$. Using this and $\mathbf{V}^{\mathrm{T}}\mathbf{V} = \mathbf{I}$, (12) can be rewritten as

$$\begin{aligned} \mathbf{P}^{\mathrm{b}} - \mathbf{P}^{\mathrm{a}} &= \left(\mathbf{U\Sigma V}(\mathbf{HX}^{\mathrm{b}})^{\mathrm{T}}\mathbf{Q}{\Lambda_o}^{-1/2}\right)\left(\mathbf{U\Sigma V}(\mathbf{HX}^{\mathrm{b}})^{\mathrm{T}}\mathbf{Q}{\Lambda_o}^{-1/2}\right)^{\mathrm{T}} \\ &= \left(\mathbf{U}\mathbf{\Sigma}^2(\mathbf{HU})^{\mathrm{T}}\mathbf{Q}{\Lambda_o}^{-1/2}\right)\left(\mathbf{U}\mathbf{\Sigma}^2(\mathbf{HU})^{\mathrm{T}}\mathbf{Q}{\Lambda_o}^{-1/2}\right)^{\mathrm{T}} \end{aligned} \tag{14}$$

Computing the trace of (14) can be further simplified. Since the columns of $\mathbf{L}$ are orthonormal, the leading multiplication by $\mathbf{L}$ in each of the factors on the r.h.s. can be omitted without changing the trace of the product, and

$$tr(\mathbf{P}^{\mathrm{b}} - \mathbf{P}^{\mathrm{a}}) = tr\left[\left(\mathbf{\Sigma}^2(\mathbf{HU})^{\mathrm{T}}\mathbf{Q}{\Lambda_o}^{-1/2}\right)\left(\mathbf{\Sigma}^2(\mathbf{HU})^{\mathrm{T}}\mathbf{Q}{\Lambda_o}^{-1/2}\right)^{\mathrm{T}}\right] \tag{15}$$

This equation is relatively inexpensive to compute. There is an up-front cost of performing an singular value decomposition of $\mathbf{P}^{\mathrm{b}}$, but this need be done only once, and after this decomposition is performed, then the evaluation of (15) at any particular observation location can be performed quickly. The operation $(\mathbf{HU})^{\mathrm{T}}$ is (for this model) simply an extraction of forecast values at observation locations from the ensemble of eigenvectors, and the multiplication by Λ_p is inexpensive since Λ_p is diagonal. An eigenvalue decomposition of $\mathbf{HP}^{\mathrm{b}}\mathbf{H}^{\mathrm{T}}$ must be performed for each potential observation location, but the rank of this matrix is relatively small, and so its decomposition is inexpensive.

Note that for computational reasons, we have made one simplification that may reduce the accuracy of this targeting scheme. Background error covariances in the targeting algorithm are assumed to be a *direct outer product* of ensemble member forecasts' deviation from their mean, as in (12); that is, $\mathbf{P}^{\mathrm{b}}$ is modeled strictly in a reduced, n-dimensional subspace to make the computations tractable. The targeting model of covariances thus assumes no localization, nor a hybridization of ensemble-based and stationary covariances; even though these features may be a part of the actual data assimilation, their inclusion would make the computations here much

more expensive. This simplifying assumption may cause some minor misestimation of the actual benefits of assimilating an observation. Results (not shown) indicated that the discrepancies introduced by making these approximations resulted only in a very small misestimation of the expected reduction in analysis variance.

c. Targeting based on maximizing the reduction of forecast error variance.

Next, consider choosing locations for additional observations with the goal of minimizing the forecast-error variance. This requires comparing the forecast from $\overline{\mathbf{x}}^{\mathrm{a}}$, the analysis including both routine and additional observations, with that from $\vec{\mathbf{x}}^{\mathrm{b}}$, the analysis based using only routine observations). Denoting quantities pertaining to these two forecasts by superscripts $f|a$ and $f|b$, respectively, the change in forecast-error variance produced by the additional observations is $tr(\mathbf{P}^{\mathrm{f|b}} - \mathbf{P}^{\mathrm{f|a}})$. Our methodology is again similar to that proposed in Bishop et al. (2001) and used in Majumdar et al. (2001).

If the analysis errors are not too large, then $\mathbf{P}^{\mathrm{f|b}} - \mathbf{P}^{\mathrm{f|a}} \approx \mathbf{M}(\mathbf{P}^{\mathrm{b}} - \mathbf{P}^{\mathrm{a}})\mathbf{M}^{\mathrm{T}}$, where $\mathbf{M}$ is the linearization of the nonlinear forecast operator M. Using (9) and writing $\mathbf{P}^{\mathrm{b}} = \mathbf{X}^{\mathrm{b}}\mathbf{X}^{\mathrm{b}^{\mathrm{T}}}$,

$$\mathbf{P}^{\mathrm{f|b}} - \mathbf{P}^{\mathrm{f|a}} \approx \mathbf{M}\mathbf{X}^{\mathrm{b}}(\mathbf{H}\mathbf{X}^{\mathrm{b}})^{\mathrm{T}}\left(\mathbf{H}\mathbf{P}^{\mathrm{b}}\mathbf{H}^{\mathrm{T}} + \mathbf{R}\right)^{-1}\mathbf{H}\mathbf{X}^{\mathrm{b}}(\mathbf{M}\mathbf{X}^{\mathrm{b}})^{\mathrm{T}}. \tag{16}$$

Now consider the ensemble of forecasts from the background ensemble, $\mathbf{x}_i^{\mathrm{f|b}} = M(\mathbf{x}_i^{\mathrm{b}})$ for $i = 1, \ldots, n$. With the same accuracy, $\mathbf{M}\mathbf{X}^{\mathrm{b}}$ in (16) can be replaced by $\mathbf{X}^{\mathrm{f|b}}$, the matrix whose ith column is $(n-1)^{-1/2}(\mathbf{x}_i^{\mathrm{f|b}} - \overline{\mathbf{x}}^{\mathrm{f|b}})$, and (16) becomes

$$\mathbf{P}^{\mathrm{f|b}} - \mathbf{P}^{\mathrm{f|a}} \approx \mathbf{X}^{\mathrm{f|b}}(\mathbf{H}\mathbf{X}^{\mathrm{b}})^{\mathrm{T}}\left(\mathbf{H}\mathbf{P}^{\mathrm{b}}\mathbf{H}^{\mathrm{T}} + \mathbf{R}\right)^{-1}(\mathbf{H}\mathbf{X}^{\mathrm{b}})\mathbf{X}^{\mathrm{f|b}^{\mathrm{T}}}. \tag{17}$$

An efficient calcuation of $tr(\mathbf{P}^{\mathrm{f|b}} - \mathbf{P}^{\mathrm{f|a}})$ now proceeds as in (14) with the eigendecomposition of $\left(\mathbf{H}\mathbf{P}^{\mathrm{b}}\mathbf{H}^{\mathrm{T}} + \mathbf{R}\right)$ and singular-value decomposition of $\mathbf{X}^{\mathrm{f|b}}$ as in (13) as

$$\mathbf{X}^{\mathrm{f|b}} = \mathbf{U}^{\mathrm{f|b}}\Sigma^{\mathrm{f|b}}\mathbf{V}^{\mathrm{f|b}^{\mathrm{T}}}. \tag{18}$$

Thus,

$$tr(\mathbf{P}^{\mathrm{f|b}} - \mathbf{P}^{\mathrm{f|a}}) = tr\left[\left(\Sigma^{\mathrm{f|b}}\mathbf{V}^{\mathrm{f|b}}(\mathbf{H}\mathbf{X}^{\mathrm{b}})^{\mathrm{T}}\mathbf{Q}{\Lambda_o}^{-1/2}\right)\left(\Sigma^{\mathrm{f|b}}\mathbf{V}^{\mathrm{f|b}}(\mathbf{H}\mathbf{X}^{\mathrm{b}})^{\mathrm{T}}\mathbf{Q}{\Lambda_o}^{-1/2}\right)^{\mathrm{T}}\right], \tag{19}$$

again omitting a factor of $\mathbf{U}^{f|b}$ that does not change the trace.

Algorithmically, the first step is to perform SVDs of the forecasts as in (18). Then for each observation location (each **H**), compute the expected reduction in forecast error variance using (19). After each **H** has been tested, the target location is determined from the **H** where the trace was largest.

4. PERFORMANCE OF THE ENSEMBLE DATA ASSIMILATION METHODS.

Before demonstrating the target selection method, we document the general performance of the three data assimilation methods using the observations at the fixed network of rawinsondes in Fig. 1. We describe the general error characteristics of each ensemble, as the error characteristics will affect the amount of improvement that can be expected from a new observation. As well, the sampling characteristics of the ensembles are briefly documented to justify using each ensemble to estimate background error covariances. In the subsequent section, the ensemble from each of three experimental data assimilation cycles will be tested for their efficacy in defining target locations using (15).

For each of the three assimilation methods, a 90-day cycle of short-range forecasts and analyses were generated here, with an updated analysis generated every 12 hours. We document the performance of three data assimilation schemes as described in Section 2b, Appendix 1, and Table 2: an "inflated" ensemble Kalman filter, a "hybrid" EnKF/3D-Var scheme, and a "perturbed observation" ensemble where the covariances are stationary, as in 3D-Var. For each experiment, a 100-member ensemble was used.

A time series of analysis errors in the total energy norm for each member and for the ensemble mean is shown in Figs. 2 a-c. As expected, for each of the three ensembles, the mean analysis is substantially lower in error than the large majority of individual ensemble member analyses. Errors for the inflated ensemble are slightly lower than for the hybrid, and both of these are dramatically lower in error than for the perturbed observation ensemble, indicating the dramatic benefits that may be achievable with accurate, flow-dependent backround error covari-

ances (though the relative improvement may be misleading of the results in real-world weather prediction, since these experiments are conducted with a relatively simple model in a perfect-model framework).

We also provide a second metric of forecast quality, measuring the ability of the ensemble to sample properly from the distribution of plausible forecast states. For a properly constructed ensemble, low analysis error should be accompanied by uniformly distributed rank histograms (Hamill 2001 and references therein). The rank of the truth relative to a sorted n-member ensemble of forecasts should be equally likely to occur in any of the n + 1 possible ranks if the truth and ensemble sample the same underlying probability distribution. Hence, over many samples, a histogram of the ranks of truth relative to the sorted ensemble should be approximately uniform.

Figures 3 a-c provides rank histograms for model level 4 potential temperature, generated using a subset of 20 times from the time series, with the first sample analysis taken 10 days after the start of the cycle and with 4 days between each sample analysis and samples taken every 250 km in the domain (see caveats in Hamill 2001 about using samples spaced this closely together). There is an excess of population at the highest ranks, more notably for the two variants of the ensemble Kalman filter. Interestingly, there appears to be more non-uniformity for the simulation where analysis errors were lower. This showed up in many other simulations as well; often lower analysis errors were accompanied by more non-uniform rank histograms, suggesting that it is difficult to optimize the ensemble simultaneously for minimum error characteristics and optimum sampling characteristics. In any case, the departures from non-uniformity are quite mild, and it should be generally reasonable to expect that the background error covariance estimates required by the targeting algorithm should be reasonably estimated by the sample covariance of the ensemble.

5. TARGETED OBSERVATION RESULTS.

a. Targeting with full algorithm

We now test the scheme that selects the target location which will maximize the expected reduction in analysis error variance (eq. 15). The targeting results shown here are primarily based on the same subset of 20 of the times in this series, starting ten days into the analysis cycle and every 4 days thereafter. The analyses produced by the assimilation of the fixed network of rawindondes (raobs) are used as the background states for the targeting tests performed here. This is a generally justifiable assumption to make if the observations are assimilated serially (Gelb 1974, Anderson and Moore 1979), though see Whitaker and Hamill (2001) for circumstances under which this approximation is not valid.

As a first check of our targeting algorithm, we assess whether the expected reduction of variance is consistent with the actual reduction in variance achieved during the data assimilation. It was assumed that a raob profile with statistics from Table 1 would be available at each of the fixed set of locations shown in Fig. 4. For each of these locations, the appropriate **H** operator was developed, and $tr(\mathbf{P}^{\mathrm{b}} - \mathbf{P}^{\mathrm{a}})$ was computed via (15). Then, for sample on each of the 20 days, $tr(\mathbf{P}^{\mathrm{b}})$ was computed in the energy norm using (1). The result of this calculation was a set of estimates of the expected reduction in the sample variance of $\mathbf{P}^{\mathrm{a}}$. The expected fractional reduction in variance

$$b = \frac{tr(\mathbf{P}^{\mathrm{b}} - \mathbf{P}^{\mathrm{a}})}{tr(\mathbf{P}^{\mathrm{b}})} \tag{20}$$

was then computed for each sample. Next, for each location and time, a sample control observation was generated, and then a set of perturbed observations. The perturbed observations were assimilated using a standard ensemble Kalman filter algorithm, with no localization of covariances, no inflation of member deviations, nor hybridization. We then computed the actual fractional reduction in variance

$$a = \frac{\frac{1}{n-1}\sum_{i=1}^{n}(\mathbf{x}_i^{\mathrm{a}} - \overline{\mathbf{x}}^{\mathrm{a}})(\mathbf{x}_i^{\mathrm{a}} - \overline{\mathbf{x}}^{\mathrm{a}})^{\mathrm{T}}}{tr(\mathbf{P}^{\mathrm{b}})} \tag{21}$$

in the energy norm from the ensemble of analyzed states. The expected fractional reduction from (20) in the sample analysis variance ought to closely match the actual reduction from (21), with minor variations due to the use of randomly perturbed observations in the actual data assimilation whose sample variance/covariance statistics may not perfectly match those used in the

data assimilation. Fig. 5(a) shows the scatterplot of the b vs. a, which as expected shows a very strong correlation.

Forecast ensembles provide an estimate of the conditional distribution of $\mathbf{x}^t$ (given all previously available observations). The sample mean is an estimate of $\mathbf{x}^t$, and the trace of the sample covariance estimates the expected squared error of mean summed over all grid pts, e.g., $||\mathbf{x}^t - \vec{\mathbf{x}}^b||^2$. Eq. (15) estimates how much the squared error of the mean is reduced from the background to the analysis by assimilating the observations. Now, we will compare that estimate in the form of b from (20) to actual reduction normalized by background error,

$$c = \frac{||\overline{\mathbf{x}}^b - \mathbf{x}^t||^2 - ||\overline{\mathbf{x}}^a - \mathbf{x}^t||^2}{||(\overline{\mathbf{x}}^b - \mathbf{x}^t)||^2}. \tag{22}$$

Using the same set of samples, Fig. 5(b) shows c plotted against b. There is much less of an obvious linear relationship, though in general large expected reductions in variance are more typically associated with large reductions in ensemble mean error. We suspect that the lack of linearity in the relationship is most likely due to the small sample size (sample points are not independent, since error structures are correlated for sample points on the same case day, and since there are only 20 case days). Also, note that 28 % of the assimilated observations actually *increased* the error.

Why do some of the assimilated observations increase the ensemble mean analysis error? (See Morss and Emanuel 2001 for an extended discussion of this topic.) First, the EnKF provides a model of background error covariances, but there is no guarantee that these error statistics are perfect. As well, the assimilated observations are imperfect, and sometimes the errors in the observations may be large enough for the observation to worsen the analysis (see Morss and Emanuel 2001, Fig. 11 for a nice illustration of this). The nature of the analysis process is of course statistical and subject to random errors; on average observations provide benefit, but they are not guaranteed to do so in every individual instance. For this perfect-model simulation with a known true state, we can assess the importance of observation errors by simply assimilating perfect observations. When they are assimilated, as shown in Fig. 6(c), only 12 % of the

instances is the mean square analysis error increased, and the magnitude of the typical degradation is significantly smaller. This suggests that the majority of the degradations were associated with errors in the observations.

Next, ensembles from each of the three data assimilation systems were used for target selection under the assumption that the ensemble could provide a perfect model of the covariances, i.e., (9) could be used instead of (8) to assess the impact if an EnKF were used for the data assimilation. The targeting algorithm (15) was used to compute $tr(\mathbf{P}^{\mathrm{b}} - \mathbf{P}^{\mathrm{a}})$ for each horizontal grid point in the domain for each of the twenty case days. Figures 6-8 provide maps of the patterns of expected fractional reduction in analysis error b from (20) on three different case days using the inflated ensemble. These three cases show days where assimilating a raob profile could be expected to produce small, moderate, and large improvements, respectively. Several interesting features are shown here. First, the difference in the expected improvement between Figs. 6(b) and 8(b) is quite dramatic; less than a 10 % improvement from assimilating a raob profile to approximately a 55 % improvement. This suggests that the algorithm may be able to define days when supplemental observations will be particularly helpful, as well as where in the domain the observation should be taken to provide the most benefit. Also note that a synthetic observation was actually assimilated in each case, with concomitant dramatic reductions in analysis variance, as illustrated in panel (c) of Figs. 6-8. These show maps of the expected improvement when the targeting algorithm was applied a second time, after the first target raob has been assimilated.

Figures 7(b) and 8(b) also suggest that an optimal targeting location may differ from that the casual user might pick from inspection of the flow on that day. In Fig. 7, the ensemble apparently was uncertain about the details of the cutoff low in the northern part of the data void more than the structure of the jet. Similarly, in Fig. 8, a sheared-out trough was apparently poorly defined. Also note that the errors between the regions of the primary and secondary maxima in Figs. 7(b) were likely to be uncorrelated, given their distance from each other and that the primary target was in a cutoff low detached from the main jet. In Fig. 7(c), after assimilation of

the primary targeted observation, most of the error variance near the target location had been eliminated, but not near the secondary location. These suggest that the targeting algorithm sometimes can define two distinct target locations without iteratively running the algorithm.

The targeting examples shown so far were generated with the inflated ensemble. Are the targets and patterns of expected improvements similar when generated from the hybrid and perturbed observation ensembles? Figures 9 (a)-(c) presents the expected improvement from the hybrid ensemble computed using (15); these panels should be compared respectively to Figs. 6, 7, and 8(b). The patterns of expected improvement were quite similar, and the target locations for the latter two cases were almost identical.

The perturbed observation ensemble was also examined. In this test, the expected improvement was evaluated using (15), so that $\hat{\mathbf{P}}^{\mathrm{b}}$ was estimated from the perturbed observation ensemble using (10). This, in essence, assumed that $\mathbf{P}^{\mathrm{b}}$ was correctly estimated from the perturbed observation ensemble, and that the subsequent data assimilation was done with the EnKF instead of 3D-Var (though, in actuality, the data assimilation did use 3D-Var). Figures 10 (a)-(c) present the expected improvements for the three case days discussed. The expected improvements that might be obtained are much larger than for the inflated and hybrid ensembles, concomitant with the variance in this ensemble being larger. The regions of large improvement are also more diffuse, indicating that the perturbed observation ensemble is generally more uncertain about the state of the atmosphere over large regions, whereas the inflated and hybrid EnKFs were able to narrow down the regions with uncertainty. Of course, one would not run a perturbed observation, 3D-Var ensemble and then switch to assimilating a targeted observation via the EnKF; presumably, 3D-Var would be used for the assimilation of the targeted observation. We will revisit shortly the impact of a targeted observation when much less accurate 3D-Var statistics are used for the data assimilation instead of the ensemble-based statistics.

However, let us briefly return to assessing the impact of these targeted observations on improving analysis errors. To assess the improvement, for each of the 20 case days, the optimal target location was determined for the inflated, hybrid, and perturbed observation ensemble us-

ing (15). Because the accuracy of the subsequent analysis may depend upon the accuracy of the observation, for each case day we generated 5 independent realizations of the control observations by adding errors to the true state, with the errors consistent with $\mathbf{R}$. Each observation was then separately assimilated using the same set of background forecasts. c and b were computed from (22) and (20), respectively, and c vs. b is plotted in Figs. 11 (a)-(c) for the inflated, hybrid, and perturbed observation ensembles, respectively using (15). The expected reduction in variance and the actual reduction in ensemble mean error were roughly consistent for the inflated and hybrid ensembles; generally, larger expected reductions in the ensemble mean error were associated with larger expected reductions in analysis variance. However, the actual reduction for the perturbed observation ensemble was much less than predicted. This, as noted in the preceding paragraph, was a consequence of the actual data assimilation being performed with 3D-Var while the targeting algorithm assumes that the assimilation was performed with an EnKF. Now, suppose that the ensemble really does provide an accurate model of $\mathbf{P}^b$, but the much less accurate 3D-Var statistics are to be used for the data assimilation. Then we can evaluate the improvement from a targeted observation based on equation (8) instead of (9); here, we compute the trace of (9) assuming $\hat{\mathbf{P}}^b$ is the stationary, 3D-Var covariance model and $\mathbf{P}^b$ is the covariance estimate from the perturbed observation ensemble. Fig. 11 (d) shows c vs. b under these assumptions. Now, the expected improvement from assimilating via 3D-Var based on (9) was consistent with the ensemble mean errors. We note that accurately evaluating the improvement from assimilating targeted observations via 3D-Var requires a reasonably perfect estimate of the background error covariances, such as may be supplied from an EnKF; if one has such an estimate and could perform the assimilation via an EnKF as readily as via 3D-Var, one might as well assimilate the data with the EnKF. Note also that greater improvements from targeted observations when using a more sophisticated data assimilation system has previously been suggested by Bergot (2000) and Bishop et al. (2001).

Consider now whether the three ensembles were picking similar target locations. Figure 9 suggests that hybrid and inflated targets were often quite similar, while Fig. 10 suggests that

perturbed observation targets were rather dissimilar. Figures 12 (a)-(b) show just how similar the targets were. The targets for the inflated and hybrid ensembles were indeed very similar (Fig. 12(a)), with the exact same target location picked on half the case days, and only three days with substantially different targets, one of which is illustrated in Figs. 6(b) and 9(a). However, when comparing the target locations from the inflated ensemble against the perturbed observation ensemble (Fig. 12(b)), there were many cases when the target locations are quite different. The differences in target locations do not necessarily indicate a problem with the perturbed observation ensemble; rather, they highlight that different data assimilation schemes will produce different estimates of the background uncertainty.

b. Improvement from targeted vs. fixed observations.

We now attempt to provide an estimate of the benefit of assimilating a supplemental targeted observation relative to assimilating a fixed observation in the middle of the void. We test this in two manners; first, we compare the analysis error reduction when either a fixed or targeted observation is intermittently assimilated. Next we consider the case if a targeted or new fixed observation replaces one of the fixed observations in the data-rich region during every data assimilation cycle.

Using the inflated ensemble and the set of 20 times used previously in Figs. 5 and 11, we applied the targeting algorithm (15). The fractional reduction in the ensemble mean analysis error c from (22) was computed and then compared to the fractional reduction that would be achieved with a fixed supplemental raob profile at the grid point (30,33), in the middle of the void. A scatterplot of the reduction is shown in Fig. 13. There is a dramatic improvement from using the targeted observation relative to the fixed observation. The mean improvement is over 20 % for the targeted observation, approximately 4.5 % for the fixed. The targeted observation improved the analysis in 19 of 20 cases vs. only 15 of 20 for the fixed.

We also performed an experiment where one observation profile in the middle of the data-rich region was removed (the observation at x=80, y=45 in Fig. 1), and either a new fixed observation at (30,33) or a targeted observation was assimilated *during every cycle.* The relative

improvement now is not nearly as dramatic (Fig. 14). There were substantial reductions in the ensemble mean analysis error from inserting a fixed observation in the middle of the void (compare to ensemble mean error of 1.07 in Fig. 2(a)). With a targeted observation, there was further improvement, but not to the extent suggested from the experiments where a targeted observation was introduced intermittently. There may be a number of factors which limit the improvement with cycled targeted observations. First, relatively quickly, the targeted observations tamp down the background variance in the data void. The primary benefit of targeted observations occurs when the background errors are quite large; then the observation has a great impact (see Morss and Emanuel 2001 as well). When a targeted observation is continually assimilated, it reduces the maximum background errors substantially, and errors are not likely to grow back to their original magnitude in the 12 h to the next assimilation cycle. Thus, in some sense a targeted observation can make subsequent targeted observations less neccessary. Another possibility is that features with high errors eventually flow near enough by the fixed observation to be effectively corrected using the EnKF covariances.

b. Targeting based on ensemble spread

The algorithm described in (15) still requires a non-negligible amount of computer wall time and involves a moderate amount of coding. Since it is theoretically justifiable based on filtering theory and requires only minor approximations, it does provide a nice baseline for the evaluation of simpler targeting schemes. We examined one such scheme, selecting a target where the spread was largest. Such a technique has been suggested in the past in Lorenz and Emanuel (1998), Morss (1998), and Morss et al. (2000). Here, we used the squared spread (the variance about the ensemble mean) of column total energy generated from the inflated ensemble and compared it to the target locations selected from (15) using the inflated ensemble. Figures 15 (a)-(c) shows the squared spread in the ensemble on the same 3 days as pictured in Figs. 6-8; note the strong correlation in the patterns of spread and the magnitudes of expected improvement in Figs. 6, 7, and 8(b). Figure 16 (a) shows the strong correspondence of locations over the 20 cases and

how the expected improvement using (15) was quite similar to the expected improvement at the at the spread target locations.

The strong correspondence was somewhat to be expected. The Kalman gain $\mathbf{K} = \mathbf{P}^{b}\mathbf{H}^{T}(\mathbf{H}\mathbf{P}^{b}\mathbf{H}^{T}+ \mathbf{R})^{-1}$ is the product of two factors. The first, $\mathbf{P}^{b}\mathbf{H}^{T}$, is the covariance between the observation location and other grid points. The second, $(\mathbf{H}\mathbf{P}^{b}\mathbf{H}^{T} + \mathbf{R})^{-1}$, accounts for the expected differences between the observation and the background, and is determined by the spread of the ensemble at the observation location. If many grid points have errors that strongly co-vary with errors at the observation site, then the observation will make large corrections to the analysis over those covarying grid points. Conversely, if the observation location is relatively uncorrelated with many other points, its domain-averaged influence is small (Berliner et al. 1999). If the amount of covariance is rather similar from grid point to grid point, then the spread in the ensemble is the primary factor in determining target location; however, if the spread is similar everywhere, the covariance will play a bigger role in determining the target location. For the intermittent assimilation of observations, the target location apparently was determined largely by the geographical variations of spread more than by the correlation structure.

To demonstrate the improvement that may be realized from the continual application of a targeting algorithm based on spread, we performed an experiment similar to the one used to generate Fig. 14. We conducted a 90-day assimilation cycle, assimilating all of the fixed observations shown in Fig. 1 except the observation at x=80, y=45. We then assimilated a replacement targeted observation at the location with maximum spread. This resulted in a reduction of ensemble mean error in the energy norm of about 18 out in the void is what was of importance more than the specific location of the observation. To test this, we performed the same experiment of removing the observation at the location with the minimum spread, but its replacement was an observation with a fixed location of x=30, y=33, near the middle of the void. The improvement for this network was about the same as with the targeted observation based on spread.

Collectively, these results suggest that intermittent targeting based on spread *generated from an appropriate ensemble* should be both useful and simple to implement. However, when cycled, the variance in the ensemble is quickly reduced and homogenized, and the spread algorithm is not very effective. Further improvements mostly depend upon the using information on the correlation structure of errors, as evidenced by the improvement noted in Fig. 14 but not in Fig. 17.

6. DISCUSSION AND CONCLUSIONS.

The underlying theory of data assimilation provides a rational basis for the selection of a targeted observation location. Under the theory, if the prior (background) error covariance is accurately modeled and depends upon the dynamics of the flow, then the effect of a targeted observation upon analysis error variance can be estimated. At first glance, the equation for estimating this posterior covariance appears computationally too demanding to be useful, owing to the high dimensionality of the background error covariance matrix. However, if background error covariances are modeled using ensemble data assimilation methods such as the EnKF, the background error covariances can be estimated in a reduced-dimension subspace and the computations made more efficient.

We demonstrated the application of an algorithm to select the optimal target location using the background error statistics from an ensemble Kalman filter in a quasigeostrophic model. The algorithm was able to determine locations on each day where a supplementary observation was of the greatest expected benefit, and it was able to determine how much this benefit changes from day to day. When tested in a simple quasigeostrophic channel model under perfect-model assumptions, the algorithm found large day-to-day variations in the expected improvement from a targeted observation, suggesting that it may be possible to define a small subset of days when such supplemental observations will be especially helpful in reducing analysis errors.

The importance of the data assimilation scheme, and a technique for accounting in the targeting algorithm for the scheme to be used to assimilate additional observations, were also tested.

Given a good estimate of the backround error covariances (from a perturbed-observation ensemble), additional observations produced a much greater reduction in error when assimilated with an EnKF than when assimilated with 3D-Var. In addition, we also showed that, by using (8), such differences among assimilation schemes could be explicitly included when selecting an optimal observation location; but application of this method still required a good estimate of the background error covariances. These results highlight the crucial need for accurate estimates of the background error covariance matrix when choosing or assimilating adaptive observations.

If a targeted observation was assimilated intermittently, that observation increased the percentage of analysis error variance reduction fourfold compared to the assimilation of an observation at a fixed location in the middle of the data void. However, if either a fixed or a targeted observation was assimilated during every data assimilation cycle, the reduction in error was less dramatic. Targeted observations were most helpful in situations when the background errors are large. Thus, if previous targeted observations had already dramatically reduced analysis errors, subsequent targeted observations were less useful.

As a proxy for the full targeting algorithm developed here, we examined the efficacy of assimilating a targeted observation based on the spread in the ensemble. If such an observation was intermittently assimilated, it provided nearly the same level of benefit as an observation taken at the location determined from the full targeting algorithm. However, if a targeted observation based on ensemble spread is assimilated every cycle, the reduction in error relative to a fixed observation was negligible. This suggests that the spread algorithm efficiently determines locations where background errors were large, and assimilation of the targeted observation significantly reduced the analysis error. However, once the background errors had been made more uniformly distributed, the spread algorithm provided little or no subsequent benefit. Likely this was because the reduction in analysis error from a given observation is both a function of the uncertainty (the spread) in background errors and the structure of how errors were correlated between the observation location and the analysis grid point. This latter effect was apparently

more important in situations where there were not dramatic spatial variations in background error statistics.

Readers are cautioned not to overinterpret the results presented here. These results used a simplified, quasigeostrophic channel model under the assumptions of no model error. Further, the network we tested had a dramatic data void; in reality, observations are available throughout the real-world data voids, though often the observations are of lesser quality and do not contain detailed vertical structure. Further, the algorithms presented here will not work as well if there is a large amount of nonlinearity in the forecast or non-Gaussianity of error distributions. Given all these qualifications, our results should be interpreted as estimating an upper bound for the usefulness of adaptive observations. Nonetheless, this algorithmic approach may be very attractive, since it is theoretically consistent with the underpinnings of current data assimilation systems.

The application of such an algorithm in real-world numerical weather prediction and data analysis presupposes the existence of an operational EnKF or other similar algorithm. While many groups are working toward this goal, as of yet there is no operational EnKF for atmospheric data assimilation. Perhaps the clear benefit of the EnKF, not only for straightforward data assimilation, but also for these ancillary applications, will make its appeal greater within the operational numerical forecast facilities.

7. APPENDIX 1: DATA ASSIMILATION METHODS.

Each of the three ensembles are generated by conducting parallel data assimilation cycles, with different member cycles receiving different perturbed observations. We start with an ensemble of n member analyses at some time t_0. These perturbed analyses were generated by adding scaled differences between random model states (Schubert and Suarez 1989) to a control analysis. We then repeat the following three-step process for each data assimilation cycle: (1) Make n forecasts to the next analysis time, here, 12 h hence. These forecasts will be used as background fields for n subsequent parallel objective analyses. (2) Given the already imperfect observations at this next analysis time (hereafter called the "control" observations), generate n in-

dependent sets of *perturbed* observations by adding random noise to the control observations. The noise is drawn from the same distributions as the observation errors (see section 2a). The perturbations are constructed in a manner to ensure that the mean of the perturbed observations is equal to the control observation. (3) Perform n objective analyses, updating each of the n background forecasts using the associated set of perturbed observations. The rationale for this methodology is outlined in Burgers et al. (1998). The details of how the objective analysis is performed for each of the three ensembles is discussed below.

Additional complexity will be introduced here to the basic design of the EnKF. As noted in previous work, (e.g., Houtekamer and Mitchell 1998, van Leeuwen 1999, Hamill et al. 2001), these details are added to simplify computations, to improve the analysis, and perhaps most importantly, to avoid the effects of a detrimental process known as "filter divergence". This is a process whereby errors can start a cyclical and worsening underestimation of background covariances that results in the ensemble ignoring the influence of new observations. A discussion of this problem is provided in Hamill et al. (2001).

A variety of methods have been tried to prevent filter divergence. Houtekamer and Mitchell (1998) and Mitchell and Houtekamer (2000) propose the use of a "double" EnKF, and more recently, a localization of ensemble covariance estimates, explained later (Houtekamer and Mitchell 2000). Anderson and Anderson (1999) suggest inflating the deviation of background members with respect to their mean by a small amount. Hamill and Snyder (2000) proposed a hybrid ensemble Kalman filter/3D-Var data assimilation system, where background error covariances are modeled as a weighted linear combination of covariances from the ensemble and stationary covariances from 3D-Var. By including a small amount of 3D-Var covariances which have more degrees of freedom and are larger in magnitude (by virtue of being a less accurate data assimilation scheme), the algorithm draws the analyses more toward the observations and adjusts them in more directions in phase space than they are in a straight EnKF. This tends to prevent filter divergence.

We have coded the assimilation algorithm here in a general manner, permitting (a) covariance localization, (b) the inflation of member deviations from their mean, and/or (c) the hybridization with or even total usage of 3D-Var covariances. However, the implementation of the hybrid as used here is somewhat different than that described in Hamill and Snyder (2000); notably though the same forecast model is used, the analysis variable is now geopotential rather than potential vorticity, and the analysis equations are solved in observation space. Also, the 3D-Var statistics are calculated in a different manner, and covariances from the ensemble are localized. More details are provided below.

Recall $\mathbf{x}_i^{\mathrm{b}}$, $i = 1, \ldots, n$ is defined as the m-dimensional model state vector for the ith member background forecast of an n-member ensemble. The state vector $\mathbf{x}$ for the QG model data assimilation system is comprised of the streamfunction at each level and grid point, and the potential temperature at each grid point of the top and bottom boundaries.

Presuming one starts with an ensemble of initial conditions generated in a rational manner, the first step in the data assimilation is to integrate an ensemble of forecasts to the next time when observations are available. If the option to inflate the ensemble is invoked, the next step is to replace the background state with a new background state inflated about the ensemble mean forecast. Background forecasts deviation from the mean are inflated by an amount r, slightly greater than 1.0:

$$\mathbf{x}_i^{\mathrm{b}} \leftarrow r\left(\mathbf{x}_i^{\mathrm{b}} - \overline{\mathbf{x}}^{\mathrm{b}}\right) + \overline{\mathbf{x}}^{\mathrm{b}}$$

Here, the operation $\leftarrow$ denotes a replacement of the previous value.

Next, following the standard EnKF formulation, each member of the ensemble is updated. The analysis equation for the ith member is

$$\mathbf{x}_i^{\mathrm{a}} = \mathbf{x}_i^{\mathrm{b}} + \hat{\mathbf{P}}^{\mathrm{b}}\mathbf{H}^{\mathrm{T}}\left[\mathbf{H}\hat{\mathbf{P}}^{\mathrm{b}}\mathbf{H}^{\mathrm{T}} + \mathbf{R}\right]^{-1}\left(\mathbf{y}_i^{\mathrm{o}} - \mathbf{H}\mathbf{x}_i^{\mathrm{b}}\right). \qquad (A1)$$

$\mathbf{x}_i^{\mathrm{a}}$ is the subsequently analyzed state. $\mathbf{y}^{\mathrm{o}}$ denotes the set of n_o control observations, with distinct perturbed observations $\mathbf{y}_i^{\mathrm{o}}$ generated for each member forecast. $\hat{\mathbf{P}}^{\mathrm{b}}$ is an approximation of the background error covariances, described below, and $\mathbf{H}$ (here assumed linear) is an operator that

converts the model state to the observation type and location. $\mathbf{R}$ is the $n_o \times n_o$ measurement error covariance matrix; that is, the observations are related to the true state $\mathbf{x}^{\mathrm{t}}$ by $\mathbf{y}^{\mathrm{o}} = \mathbf{H}\mathbf{x}^{\mathrm{t}} + \epsilon$, where ϵ is a normally distributed, random vector with zero mean and covariance matrix $\mathbf{R}$. Note also that the operation sequence $\hat{\mathbf{P}}^{\mathrm{b}}\mathbf{H}^{\mathrm{T}}\left[\mathbf{H}\hat{\mathbf{P}}^{\mathrm{b}}\mathbf{H}^{\mathrm{T}} + \mathbf{R}\right]^{-1}$ is often referred to as the *gain matrix*; it represents how the observation increment $\mathbf{y}_i^{\mathrm{o}} - \mathbf{H}\mathbf{x}_i^{\mathrm{b}}$ will change the background state at every grid point.

In this data assimilation scheme, n_r individual fixed location raob profiles are assimilated serially; that is, the set of analyses generated by updating the background states with the first raob serves as the background states for assimilation of the second raob, and so on, until all n_r profiles are assimilated. Then these member analyses are used as the background forecasts for assimilation of a targeted observation. Because raob errors should be independent of each other, the analysis produced by the serial assimilation of raobs should be identical to the analysis produced by assimilating all raobs together (Anderson and Moore 1979). Further, this makes the rank of $\left[\mathbf{H}\hat{\mathbf{P}}^{\mathrm{b}}\mathbf{H}^{\mathrm{T}} + \mathbf{R}\right]$ rather low, so computation of its inverse is not expensive.

As in Evensen (1994) and Houtekamer and Mitchell (1998, 2001), for computational efficiency, the matrix operations $\hat{\mathbf{P}}^{\mathrm{b}}\mathbf{H}^{\mathrm{T}}$ and $\mathbf{H}\hat{\mathbf{P}}^{\mathrm{b}}\mathbf{H}^{\mathrm{T}}$ in (2) are computed together using data from the ensemble of background states. Again, $\mathbf{X}^{\mathrm{b}}$ is the matrix whose ith column is $(n-1)^{-1/2}(\mathbf{x}_i^{\mathrm{b}} - \overrightarrow{\mathbf{x}}^{\mathrm{b}})$. Then

$$\hat{\mathbf{P}}^{\mathrm{b}}\mathbf{H}^{\mathrm{T}} = \left(1-\alpha\right)\rho \circ \mathbf{X}^{\mathrm{b}}(\mathbf{H}\mathbf{X}^{\mathrm{b}})^{\mathrm{T}} + \alpha c \left\langle \hat{\mathbf{P}}^{\mathrm{b}}\mathbf{H}^{\mathrm{T}} \right\rangle, \qquad (A2)$$

and

$$\mathbf{H}\hat{\mathbf{P}}^{\mathrm{b}}\mathbf{H}^{\mathrm{T}} = \left(1-\alpha\right)\mathbf{H}\mathbf{X}^{\mathrm{b}}(\mathbf{H}\mathbf{X}^{\mathrm{b}})^{\mathrm{T}} + \alpha c \left\langle \mathbf{H}\hat{\mathbf{P}}^{\mathrm{b}}\mathbf{H}^{\mathrm{T}} \right\rangle. \qquad (A3)$$

There are two terms in each equation. The first term reprents the contribution of flow-dependent statistics derived from the ensemble, and the second term represents the stationary, 3D-Var contribution. They are weighted by α, a tuneable, fixed constant, $0.0 \leq \alpha \leq 1.0$. $\left\langle \hat{\mathbf{P}}^{\mathrm{b}}\mathbf{H}^{\mathrm{T}} \right\rangle$ and $\left\langle \mathbf{H}\hat{\mathbf{P}}^{\mathrm{b}}\mathbf{H}^{\mathrm{T}} \right\rangle$ represent time-averaged covariance information, developed from a background forecasts from a 400-member EnKF over a 90-day integration with updates every 12 h. For this implementation, the time-average covariances are calculated separately for each raob location, and

covariances need not be isotropic and may vary with the observation location. c is an inflation factor for time-averaged covariances, here set to 16.0. Various magnitudes were tested in a control 3D-Var assimilation cycle with $\alpha = 1.0$; 16.0 was found to be an approximately optimal inflation factor. This factor is larger than 1.0 since the time-averaged model for covariances is much less accurate than the flow-dependent model, so when cycled for a long time, background errors become much greater than in they are in the EnKF (see section 4 also).

The operation $\rho \circ$ in (A2) denotes a Schur product (an element-by-element multiplication) of a correlation matrix **S** with the covariance model generated by the ensemble, that is, a localization of covariances. The Schur product of matrices **A** and **B** is a matrix **C** of the same dimension, where $C_{ij} = A_{ij}B_{ij}$. For serial data assimilation, the function **S** depends upon the observation location; it is a maximum of 1.0 at the observation location and typically decreases montonically to zero at some finite distance from the observation. The Schur product is not applied in (A3), a minor approximation; the **H** operator involves a limited stencil of grid points near the observation location, and the correlation at all grid points is approximately 1.0. See Houtekamer and Mitchell (2001) and Hamill et al. (2001) for further explanations of the rationale for covariance localization.

Because the forecast model we use has impermeable walls on the north and south walls, **S** cannot be modeled strictly using a simple isotropic localization function around the observation such as suggested by Gaspari and Cohn (1999); the Schur product of this with $\hat{\mathbf{P}}^{\mathrm{b}}\mathbf{H}^{\mathrm{T}}$ will produce different elements in the gain matrix for the grid points along the north and south walls. This in turn will cause analysis increments to vary along the walls, producing a model state which violates the boundary conditions. Hence, a modified form of covariance localization is used that permits the same covariance value to be used at all points along the wall.

To localize covariances, we use the compactly supported, 5th-order function in Gaspari and Cohn (1999). Define a correlation length scale l_c, measured in model grid points, and let $F_c = \sqrt{\frac{10}{3}}\, l_c$. Define $||D_{ij}||$ to be the Euclidean distance in grid points between grid point (i, j) and the observation location. Then an isotropic localization function w_{ij} is defined for every grid

point (i, j) in the domain according to $w_{ij}(i, j) = \mathbf{\Omega}\,(F_c, ||D_{ij}||)$, where

$$\mathbf{\Omega}\,(a, b) = \begin{cases} -\frac{1}{4}\left(\frac{b}{a}\right)^5 + \frac{1}{2}\left(\frac{b}{a}\right)^4 + \frac{5}{8}\left(\frac{b}{a}\right)^3 - \frac{5}{3}\left(\frac{b}{a}\right)^2, & 0 \leq b \leq a; \\ \frac{1}{12}\left(\frac{b}{a}\right)^5 - \frac{1}{2}\left(\frac{b}{a}\right)^4 + \frac{5}{8}\left(\frac{b}{a}\right)^3 + \frac{5}{3}\left(\frac{b}{a}\right)^2 - 5\left(\frac{b}{a}\right) + 4 - \frac{2}{3}\left(\frac{b}{a}\right)^{-1}, & a < b \leq 2a; \\ 0. & b > 2a. \end{cases} \quad (A4)$$

We also define a function $w_j(j)$, which is maximized at the walls and decreases quickly toward zero away from them. Let n_j equal the number of grid points in north-south direction (here, 65). Define a distance from the nearest wall $||D_j||$ according to

$$||D_j|| = \begin{cases} j - 1, & \text{if } j \leq \frac{n_j}{2} + 1; \\ n_j + 1 - j, & \text{otherwise.} \end{cases} \quad (A5)$$

Then $w_j(j) = \mathbf{\Omega}\,(2.5, ||D_j||)$. Finally, we define the overall localization matrix operator **S** with element s_{ij} at the (i, j)th grid point. s_{ij} is a combination of the isotropic function and the zonally averaged function, with the weight given to each depending on j:

$$s_{ij} = \max_i\Big(w_{ij}(i, j)\Big)\,w_j(j) + \Big(1 - w_j(j)\Big)\,w_{ij}(i, j) \quad (A6)$$

Examples of what this localization function looks like for a grid point in the center of the domain and near a wall are shown in Figs. 18 a-b.

8. ACKNOWLEDGMENTS

This research was started with support through NCAR's U. S. Weather Research Program and finished at the Climate Diagnostics Center (CDC). CDC is thanked thanked for allowing the lead author to complete this research. We thank Rebecca Morss (NCAR/ASP) and Craig Bishop for their advice and detailed reviews of a draft of the manuscript, and we thank Jeff Whitaker for his extensive consultations.

REFERENCES

Anderson, B. D., and J. B. Moore, 1979: *Optimal filtering.* Prentice-Hall, Inc., 357 pp.

Anderson, J. L., and S. L. Anderson, 1999: A Monte Carlo implementation of the nonlinear filtering problem to produce ensemble assimilations and forecasts. *Mon. Wea. Rev.,* **127**, 2741-2758.

———, 2001: An ensemble adjustment filter for data assimilation. *Mon. Wea. Rev.*, conditionally accepted.

Baker, N. L, and R. Daley, 2000: Observation and background adjoint sensitivity in the adaptive observation-targeting problem. *Quart. J. Roy. Meteor. Soc.,* **126**, 1431-1454.

Barkmeijer, J., M. van Gijzen, and F. Bouttier, 1998: Singular vectors and estimates of the analysis error covariance metric. *Quart. J. Roy. Meteor. Soc.,* **124**, 1695-1713.

Berliner, L. M., Z.-Q. Lu, and C. Snyder, 1999: Statistical design for adaptive weather observations. *J. Atmos. Sci.,* **56**, 2536-2552.

Bergot, T., G. Hello, A. Joly, and S. Malardel, 1999: Adaptive observations: a feasibility study. *Mon. Wea. Rev.,* , **127**, 743-765.

———, 2001: Influence of the assimilation scheme on the efficiency of adaptive observations. *Quart. J. Roy. Meteor. Soc.*, in press.

Bishop, C. H., and Z. Toth, 1999: Ensemble transformation and adaptive observations. *J. Atmos. Sci.,* **56**, 1748-1765.

Bishop, C. H., B. J. Etherton, and S. Majumjar, 2001: Adaptive sampling with the ensemble transform Kalman filter. Part 1: Theoretical aspects. *Mon. Wea. Rev.,* **129**, 420-436.

Buizza, R., and A. Montani, 1999: Targeting observations using singular vectors. *J. Atmos. Sci.*, **56**, 2965-2985.

Burgers, G., P. J. van Leeuwen, and G. Evensen, 1998: Analysis scheme in the ensemble Kalman filter. *Mon. Wea. Rev.,* **126**, 1719-1724.

Cohn, S. E., 1997: An introduction to estimation theory. *J. Meteor. Soc. Jap.,* **75(1B)**, 257-288.

Ehrendorfer, M. , and J. J. Tribbia, 1997: Optimal prediction of forecast error covariances through singular vectors. *J. Atmos. Sci.*, **54**, 286-313.

Emanuel, K. A., and Coauthors, 1995: Report of the first prospectus development team of the U. S. weather research program to NOAA and the NSF, *Bull. Amer. Meteor. Soc.*, **76**, 1194-1208.

——— , and R. Langland, 1998: FASTEX adaptive observations workshop. *Bull. Amer. Meteor. Soc.*, **79**, 1915-1919.

Evensen, G., 1994: Sequential data assimilation with a nonlinear quasigeostrophic model using Monte Carlo methods to forecast error statistics. *J. Geophys. Res.*, **99 (C5)**, 10143-10162.

——— , and P. J. van Leeuwen, 1996: Assimilation of Geosat altimeter data for the Agulhas current using the ensemble Kalman filter with a quasigeostrophic model. *Mon. Wea. Rev.*, **124**, 85-96.

Gaspari, G., and S. E. Cohn, 1999: Construction of correlation functions in two and three dimensions. *Quart. J. Roy. Meteor. Soc.*, **125**, 723-757.

Gelaro, R., Langland, R., Rohaly, G.D., and T. E. Rosmond, 1999: An assessment of the singular vector approach to targeted observations using the FASTEX data set. *Quart. J. Roy. Meteor. Soc.*, **125**, 3299-3327.

——— , C. A. Reynolds, R. H. Langland, and G. D. Rohaly, 2000: A predictability study using geostationary satellite wind observations during NORPEX. *Mon. Wea. Rev.*, **128**, 3789-3807.

Gelb, A. (ed.), 1974: *Applied optimal estimation.* MIT Press, 374 pp.

Hamill, T. M., C. Snyder, and R. E. Morss, 2000: A comparison of probabilistic forecasts from bred, singular vector, and perturbed observation ensembles. *Mon. Wea. Rev.*, **128**, 1835-1851.

——— , and ——— , 2000. A hybrid ensemble Kalman filter- 3d variational analysis scheme. *Mon. Wea. Rev.*, **128**, 2905-2919.

——— , ——— , and J. S. Whitaker, 2001: Distance-dependent filtering of background error covariance estimates in an ensemble Kalman filter. *Mon. Wea. Rev.*, accepted. Available from www.cdc.noaa.gov/∼hamill

——— , 2001: Interpretation of rank histograms for verifying ensemble forecasts. *Mon. Wea. Rev.*, **129**, 550-560.

Hansen, J. A., and L. A. Smith, 2000: The role of operational constraints in selecting supplementary observations. *J. Atmos. Sci.*, **57**, 2859-2871.

Houtekamer, P. L., and J. Derome, 1995: Methods for ensemble prediction. *Mon. Wea. Rev.*, **123**, 2181-2196.

——— , and H. L. Mitchell, 1998: Data assimilation using an ensemble Kalman filter technique. *Mon. Wea. Rev.*, **126**, 796-811.

——— , and ——— , 2001: A sequential ensemble Kalman filter for atmospheric data assimilation. *Mon. Wea. Rev.*, **129**, 123-137.

Ide, K., P. Courtier, M. Ghil, and A. C. Lorenc, 1997: Unified notation for data assimilation: operational, sequential, and variational. *J. Meteor. Soc. Jap.*, **75 (1B)**, 181-189.

Joly, A., and Coauthors, 1997: The Fronts and Atlantic Storm-track Experiment (FASTEX): scientific objectives and experimental design. *Bull. Amer. Meteor. Soc.*, **78**, 1917-1940.

Keppenne, C. L., 2000: Data assimilation into a primitive-equation model with a parallel ensemble Kalman filter. *Mon. Wea. Rev.*, **128**, 1971-1981.

Langland, R. , Z. Toth, R. Gelaro, I. Szunyogh, M. A. Shapiro, S. J. Majumdar, R. E. Morss, G. D. Rohaly, C. Velden, N. Bond, and C. H. Bishop, 1999a: The North Pacific Experiment (NORPEX-98): targeted observations for improved North American weather forecasts. *Bull. Amer. Meteor. Soc.*, **80**, 1363-1384.

——— , R. Gelaro, G. D. Rohaly, and M. A. Shapiro, 1999b: Targeted observations in FASTEX: adjoint based Targeting procedures and data impact experiments in IOP/7 and IOP/8. *Quart. J. Roy. Meteor. Soc.*, **125**, 3241-3270.

Le Dimet, F.-X., and O. Talagrand, 1986: Variational algorithms for analysis and assimilation of meteorological observations: theoretical aspects. *Tellus*, A, **38**, 97-110.

Lermusiaux, P. F. J., and A. R. Robinson, 1999: Data assimilation via error subspace statistical estimation. *Mon. Wea. Rev.*, **127**, 1385-1407.

Lorenc, A. C., 1986: Analysis methods for numerical weather prediction. *Quart. J. Roy. Meteor. Soc.*, **112**, 1177-1194.

Lorenz, E. N., and K. A. Emanuel, 1998: Optimal sites for supplementary observations: simulation with a small model. *J. Atmos. Sci.*, **55**, 399-414.

Lu, Z.-Q., L. M. Berliner, and C. Snyder, 2000: Experimental design for spatial and adaptive observations, *Studies in the Atmospheric Sciences*, L. M. Berliner, D. Nychka and T. Hoar, eds., Lecture Notes in Statistics, 144, Springer-Verlag, pp 199.

Majumdar, S.J., C.H. Bishop, I. Szunyogh, and Z. Toth, 2001: Can an Ensemble Transform Kalman Filter predict the reduction in forecast error variance produced by targeted observations? *Quart. J. Roy. Meteor. Soc.*, , submitted.

Mitchell, H. L., and P. L. Houtekamer, 2000: An adaptive ensemble Kalman filter. *Mon. Wea. Rev.*, **128**, 416-433.

Morss, R. E., 1998: *Adaptive observations: Idealized sampling strategies for improving numerical weather prediction.* Ph.D Dissertation, Massachusetts Institute of Technology. Available from UMI Dissertation Services, P. O. Box 1346, 300 N. Zeeb Rd., Ann Arbor, MI, 48106-1346. 225 pp.

——— , and K. A. Emanuel, 2001: Influence of added observations on analysis and forecast errors. *Quart. J. Roy. Meteor. Soc.*, in press.

——— , ——— , and C. Snyder, 2001: Idealized adaptive observation strategies for improving numerical weather prediction. *J. Atmos. Sci.*, **58**, 210-234.

Palmer, T. N., R. Gelaro, J. Barkmeijer, and R. Buizza, 1998: Singular vectors, metrics, and adaptive observations. *J. Atmos. Sci.*, **55**, 633-653.

Parrish, D. F., and J. C. Derber, 1992L The National Meteorological Center's spectral statistical interpolation system. *Mon. Wea. Rev.,* **120**, 1747-1763.

Pu, Z.-X., E. Kalnay, J. Sela, and I. Szunyogh, 1997: Sensitivity of forecast errors to initial conditions with a quasi-inverse linear method. *Mon. Wea. Rev.,* **125**, 2479-2503.

——— , S. J. Lord, and E. Kalnay, 1998: Forecast sensitivity with dropwindsonde data and targeted observations. *Tellus,* **50a**, 391-410.

——— , and E. Kalnay, 1999: Targeting observations with the quasi- linear inverse and adjoing NCEP global models: performance during FASTEX. *Quart. J. Roy. Meteor. Soc.,* **125**, 3329-3337.

Rabier, F., J.-N. Thepaut, and P. Courtier, 1998: Extended assimilation and forecast experiments with a four-dimensional variational assimilation system. *Quart. J. Roy. Meteor. Soc.,* **124**, 1-39.

Schubert, S. D., and M. Suarez, 1989: Dynamical predictability in a simple general circulation model: average error growth. *J. Atmos. Sci.,* **46**, 353-370.

Snyder, C., 1996: Summary of an informal workshop on adaptive observations and FASTEX. *Bull. Amer. Meteor. Soc.,* **77**, 953-965.

Snyder, C., T. M. Hamill, and S. Trier, 2001: Dynamics and statistics of analysis errors in a quasi-geostrophic model. Part I: dynamics. In preparation.

Szunyogh, I., Z. Toth, K. A. Emanuel, C. H. Bishop, C. Snyder, R. E. Morss, J. Woolen, and T. Marchok, 1999: Ensemble based targeting experiments during FASTEX: the impact of dropsonde data from the Lear jet. *Quart. J. Roy. Meteor. Soc.,* **125**, 2189-3218.

Szunyogh, I., Z. Toth, R. E. Morss, S. Majumdar, B. J. Etherton, and C.H. Bishop, 2000: The effect of targeted dropsonde observations during the 1999 Winter Storms Reconaissance Program. *Mon. Wea. Rev.,* **128**, 3520-3537.

van Leeuwen, P.J., 1999: Comment on "Data assimilation using an ensemble Kalman filter technique." *Mon. Wea. Rev.,* **127**, 1374-1377.

Whitaker, J. S., and T. M. Hamill, 2001: Ensemble data assimilation without perturbed observations. *Mon. Wea. Rev.*, submitted. Available from jsw@cdc.noaa.gov.

Yagyu, T., J. Wackermann, T. Kinoshita, T. Hirota, K. Kochi, I. Kondakor, T. Koenig, and D. Lehmann, 1997: Chewing-gum flavor affects measures of global complexity of multichannel EEG. *Neuropsychobiology*, **35**, 46-50.

FIGURE CAPTIONS

Figure 1. Location of fixed raobs for network with data void.

Figure 2. Time series of analysis errors for ensemble assimilating raob data using the fixed network in Fig. 1. Dots indicate errors of individual ensemble members, and the solid line the error of the ensemble mean. Time averaged errors for individual members and for ensemble mean are denoted by the numbers on right-hand side of plot. (a) Inflated EnKF, (b) hybrid EnKF/3D-Var, and (c) perturbed observation / 3D-Var ensemble.

Figure 3. Rank histograms for analyzed θ at model level 4. (a) Inflated ensemble, (b) hybrid, (c) perturbed observation.

Figure 4. Observation locations for testing of expected vs. actual analysis variance reduction.

Figure 5. Comparisons of variances when assimilating observations at locations in Fig. 5 using inflated ensemble. (a) Actual fractional reduction in analysis variance a vs. expected reduction in analysis variance b. (b) Fractional reduction in ensemble mean variance c vs. b when using imperfect observations, and (c) as in (b), but using perfect observations.

Figure 6. Expected reduction in analysis error variance b from application of targeting algorithm on Day 14 of the 90-day integration of the inflated ensemble assimilation scheme. (a) True geopotential height (solid) at model level 8 and θ_{T} (potential temperature on top lid; dashed). (b) Expected fractional reduction in analysis error variance from background variance b mapped for each potential observation location in the domain. Dots indicate locations of fixed network of observations previously assimilated. Star indicates location of maximum expected reduction (the target location). Contours at 2 % and every 4 % thereafter. (c) As in (b), but the improvement after the first targeted observation has been assimilated.

Figure 7. As in Fig. 7, but for day 54.

Figure 8. As in Fig. 7, but for day 70.

Figure 9. (a) As in Fig. 6(b), but for hybrid ensemble, (b) As in Fig. 7(b), but for hybrid ensemble, and (c) As in Fig. 8(b), but for hybrid ensemble.

Figure 10. (a) As in Fig. 6(b), but for perturbed observation ensemble. However, contour interval is changed to 4 % and every 8 % thereafter. (b) As in Fig. 7(b), but for perturbed observation ensemble, and (c) As in Fig. 8(b), but for perturbed observation ensemble.

Figure 11. (a) Actual fractional reduction in ensemble mean variance c vs expected fractional reduction in analysis error variance b for optimal target locations from inflated ensemble. Five independent control observations tested for each of the 20 case days. (b) As in (a), but for hybrid ensemble, and (c) As in (a), but for perturbed observation ensemble. (d) As in (c), but where eq. (9) is used instead of (10) to predict expected improvement.

Figure 12. (a) Difference in selected optimal target locations when using inflated ensemble (darkened dots) and hybrid ensemble (diamonds). Darkened diamonds indicate that target locations were identical. Targets for the same case day are connected by solid line. (b) As in (a), but for inflated ensemble vs. perturbed observation ensemble.

Figure 13. Improvement in ensemble mean analysis error when assimilating targeted vs fixed observations on each of 20 case days.

Figure 14. Time series of ensemble mean analysis errors when replacing observation profile at (80,45) in the data assimilation cycle with either a fixed profile at (30,33) or a targeted observation.

Figure 15. Squared spread in column total energy from the inflated ensemble (shaded) and level 8 geopotential (dark solid lines). Target locations are marked with a star. Contours for spread at 1, 2, 3, 5, 10, 15, 20, 30, 40, 50, and 60 $m^2 s^{-2}$. (a) Case day 14 (compare with Fig. 7b). (b) Case day 54 (compare with Fig. 8b). (c) Case day 70 (compare with Fig. 9b).

Figure 16. (a) Difference in selected optimal target locations when using full targeting algorithm with inflated ensemble (darkened dots) and targets based on maximum column total energy spread in inflated ensemble (diamonds). (b) Expected reduction in analysis error variance as evaluated from ensemble when targets locations are defined by full algorithm (abscissa) vs. at locations with maximum spread (ordinate).

Figure 17. Ensemble mean errors in the energy norm using the inflated ensemble. Solid line indicates errors for where a single sounding from the fixed network at the location x=80,y=45 has been replaced by a sounding at a sounding at x=30, y=33. Dashed line indicates errors where sounding at x=80,y=45 is replaced by a targeted observation with the location determined by the maximum spread.

Figure 18. Covariance localization functions for (a) grid point near the center of the channel, and (b) grid point near wall. Correlation length scale in this example is 15 grid points.

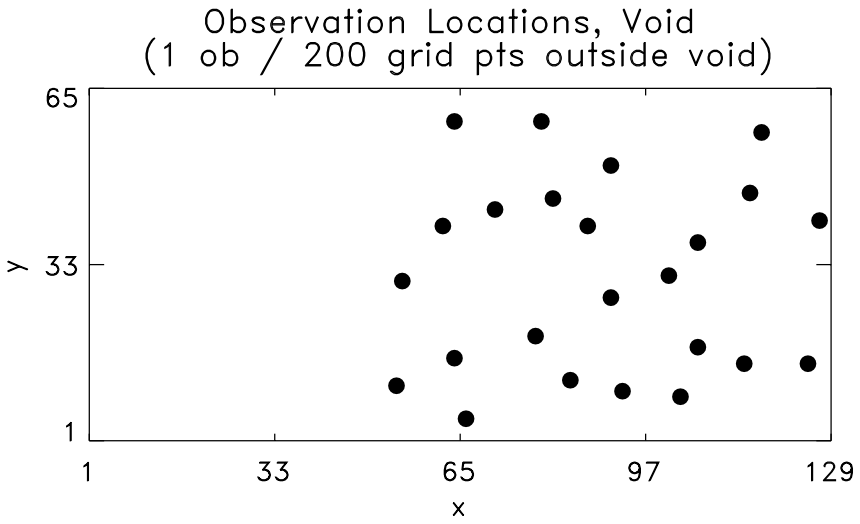

Figure 1. Location of fixed raobs for network with data void.

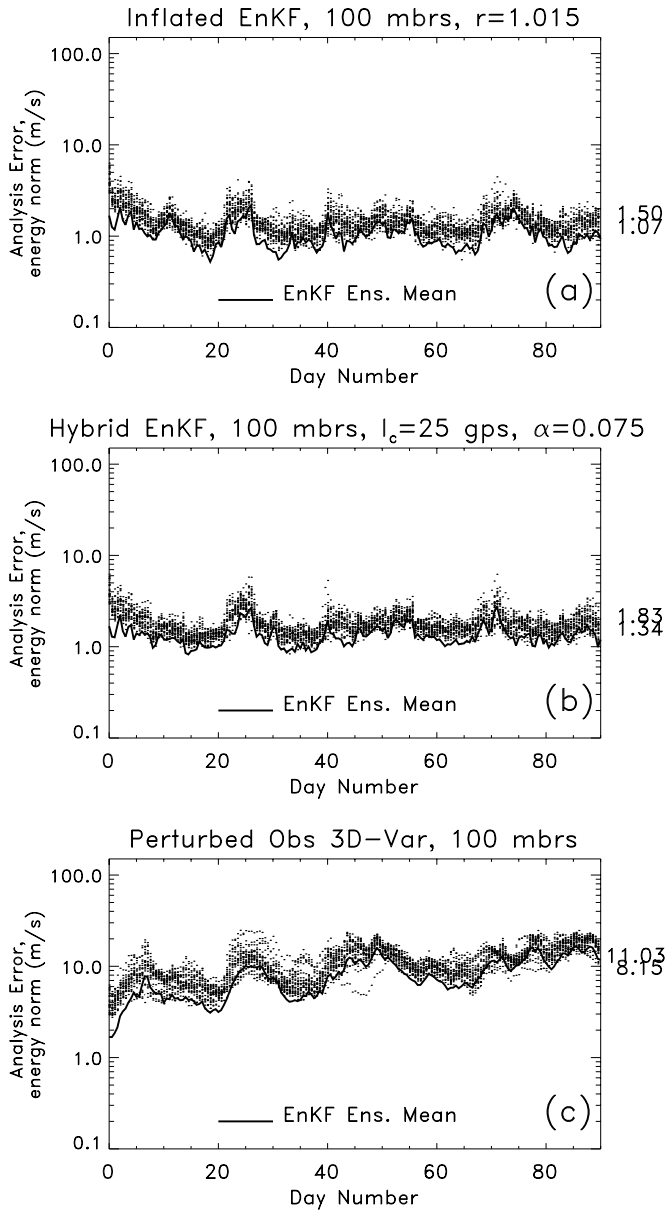

Figure 2. Time series of analysis errors for ensemble assimilating raob data using the fixed network in Fig. 1. Dots indicate errors of individual ensemble members, and the solid line the error of the ensemble mean. Time averaged errors for individual members and for ensemble mean are denoted by the numbers on right-hand side of plot. (a) Inflated EnKF, (b) hybrid EnKF/3D-Var, and (c) perturbed observation / 3D-Var ensemble.

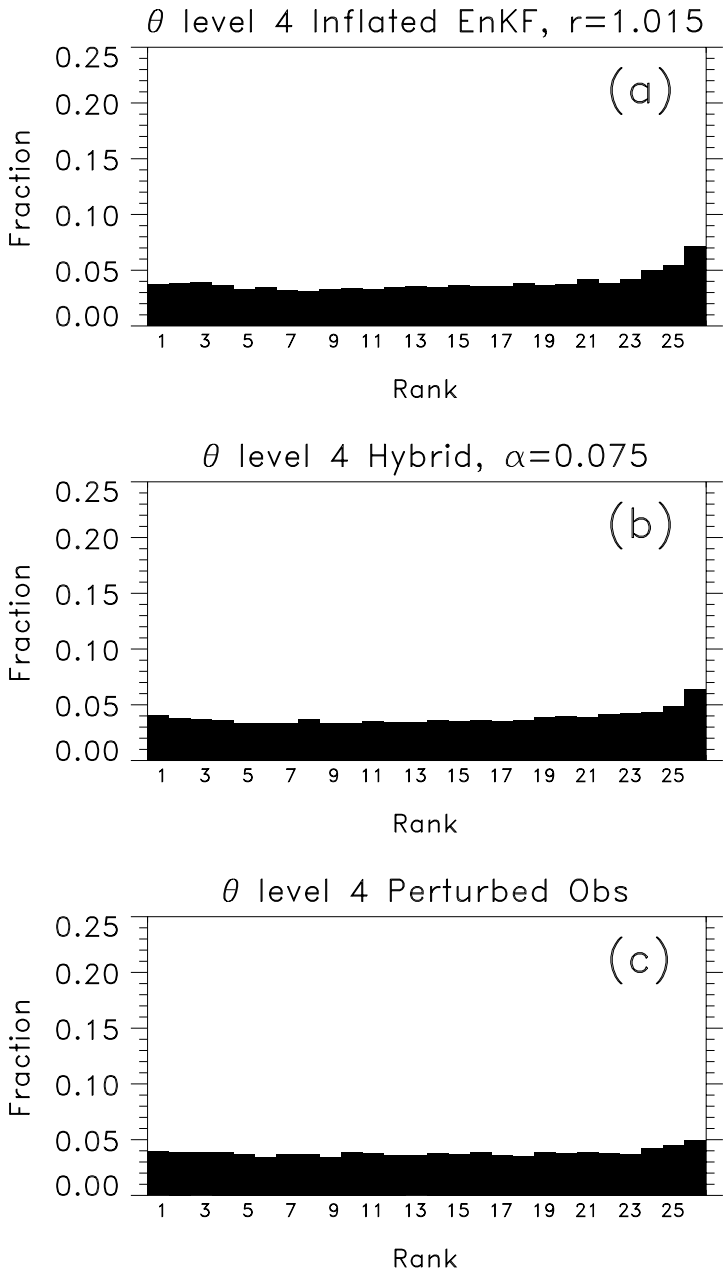

Figure 3. Rank histograms for analyzed θ at model level 4. (a) Inflated ensemble, (b) hybrid, (c) perturbed observation.

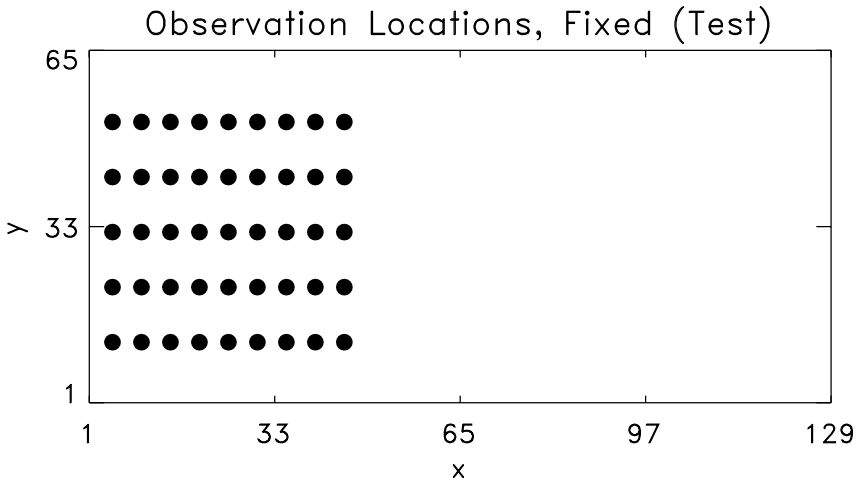

Figure 4. Observation locations for testing of expected vs. actual analysis variance reduction.

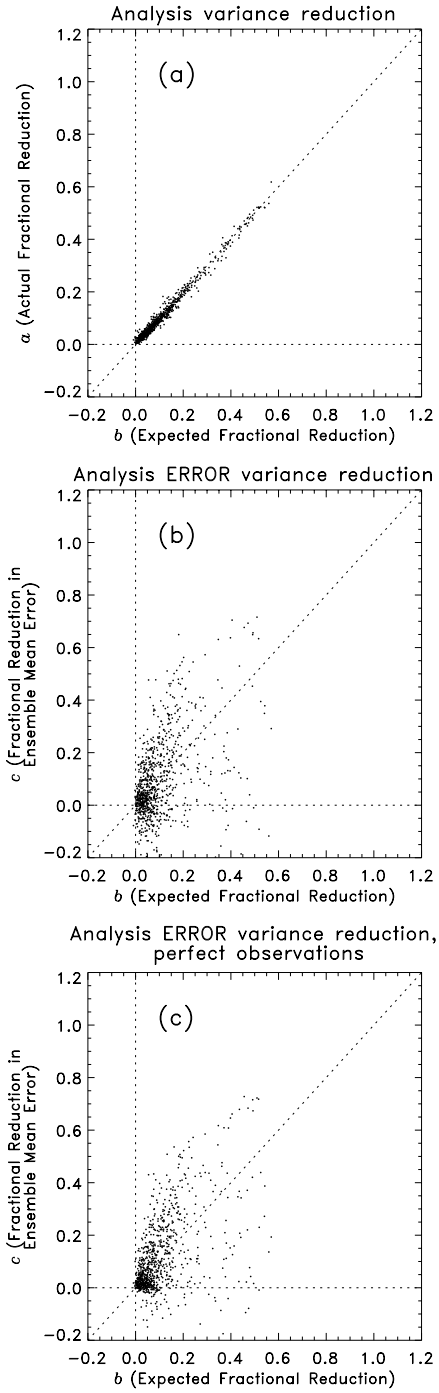

Figure 5. Comparisons of variances when assimilating observations at locations in Fig. 5 using inflated ensemble. (a) Actual fractional reduction in analysis variance a vs. expected reduction in analysis variance b. (b) Fractional reduction in ensemble mean variance c vs. b when using imperfect observations, and (c) as in (b), but using perfect observations.

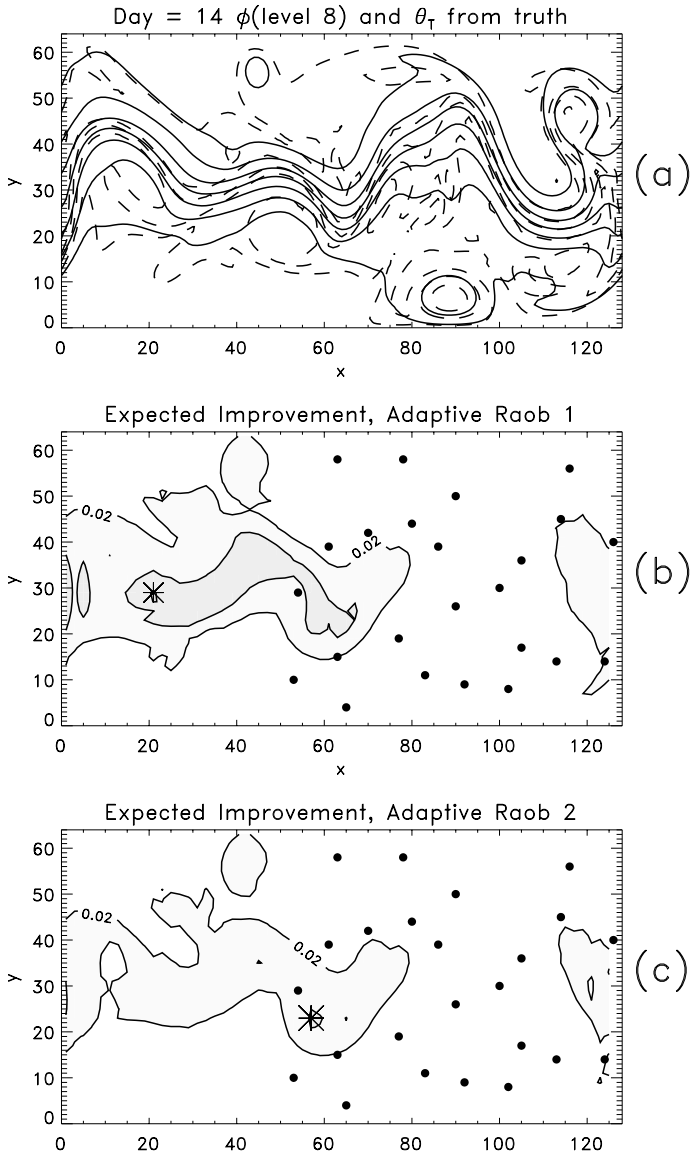

Figure 6. Expected reduction in analysis error variance b from application of targeting algorithm on Day 14 of the 90-day integration of the inflated ensemble assimilation scheme. (a) True geopotential height (solid) at model level 8 and θ_T (potential temperature on top lid; dashed). (b) Expected fractional reduction in analysis error variance from background variance b mapped for each potential observation location in the domain. Dots indicate locations of fixed network of observations previously assimilated. Star indicates location of maximum expected reduction (the target location). Contours at 2 % and every 4 % thereafter. (c) As in (b), but the improvement after the first targeted observation has been assimilated.

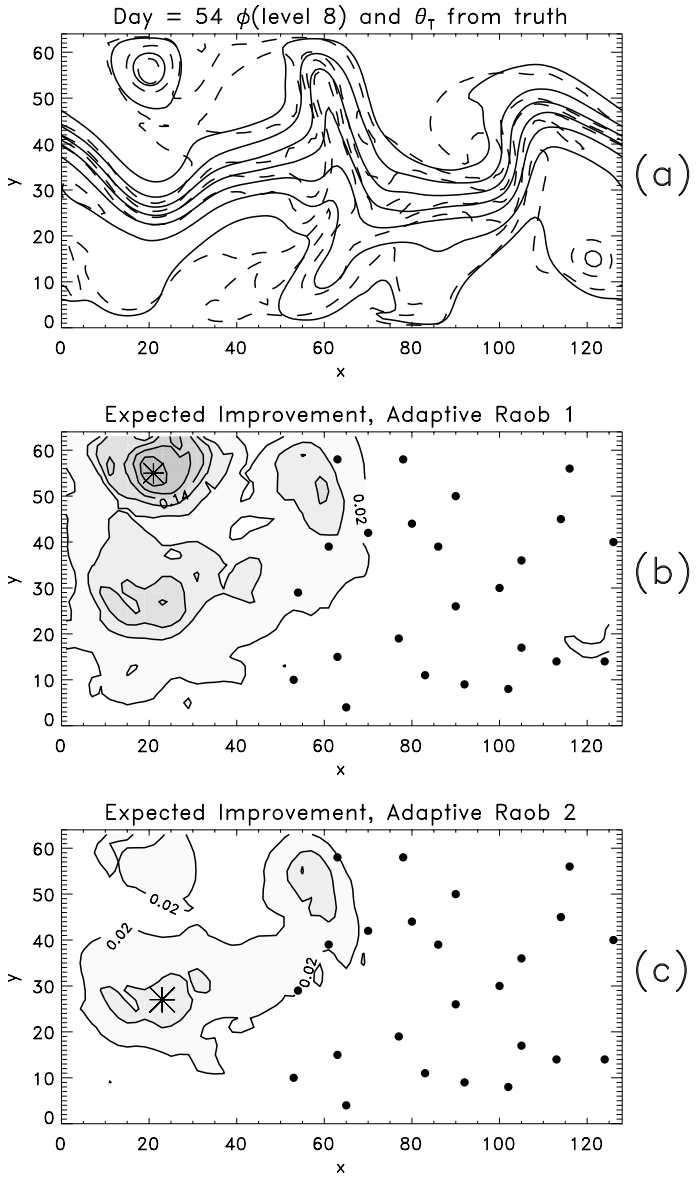

Figure 7. As in Fig. 7, but for day 54.

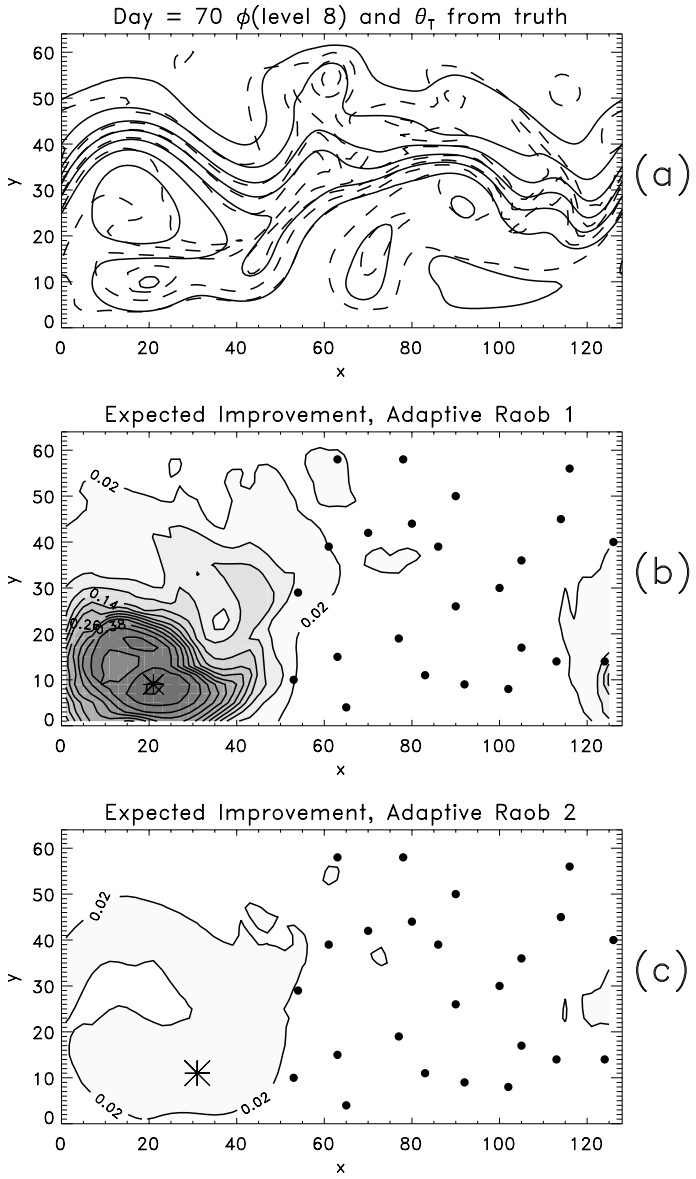

Figure 8. As in Fig. 7, but for day 70.

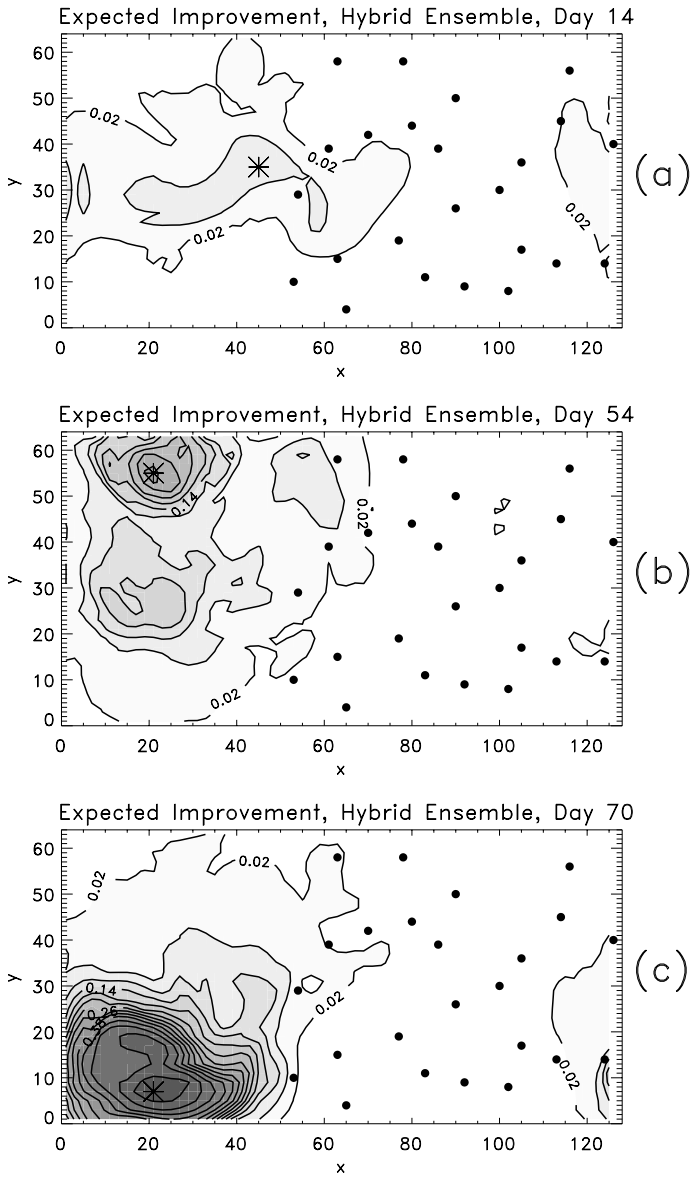

Figure 9. (a) As in Fig. 6(b), but for hybrid ensemble, (b) As in Fig. 7(b), but for hybrid ensemble, and (c) As in Fig. 8(b), but for hybrid ensemble.

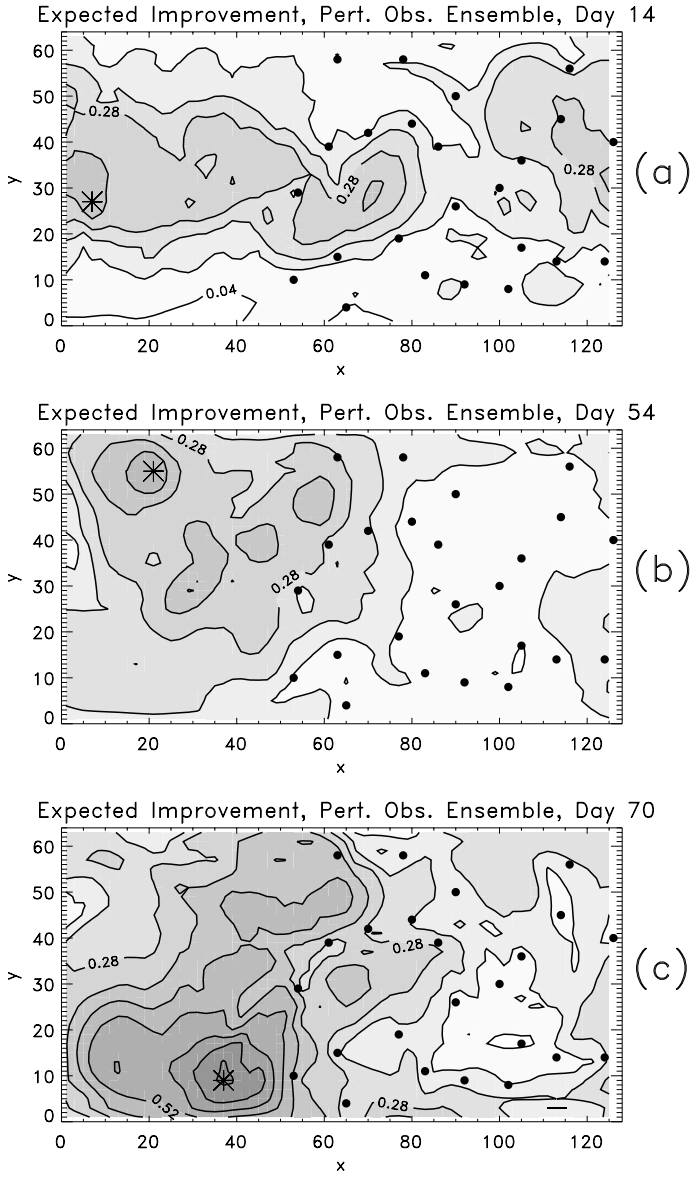

Figure 10. (a) As in Fig. 6(b), but for perturbed observation ensemble. However, contour interval is changed to 4 % and every 8 % thereafter. (b) As in Fig. 7(b), but for perturbed observation ensemble, and (c) As in Fig. 8(b), but for perturbed observation ensemble.

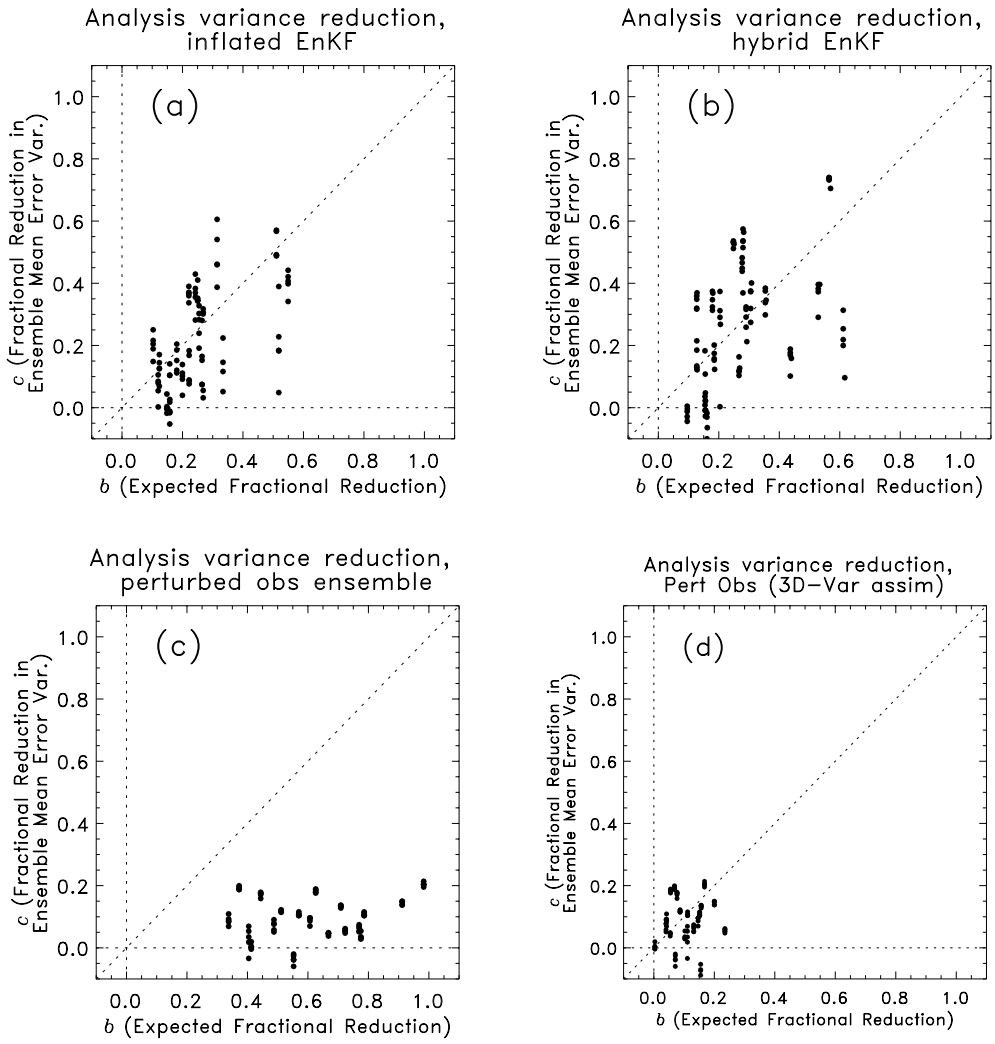

Figure 11. (a) Actual fractional reduction in ensemble mean variance c vs expected fractional reduction in analysis error variance b for optimal target locations from inflated ensemble. Five independent control observations tested for each of the 20 case days. (b) As in (a), but for hybrid ensemble, and (c) As in (a), but for perturbed observation ensemble. (d) As in (c), but where eq. (9) is used instead of (10) to predict expected improvement.

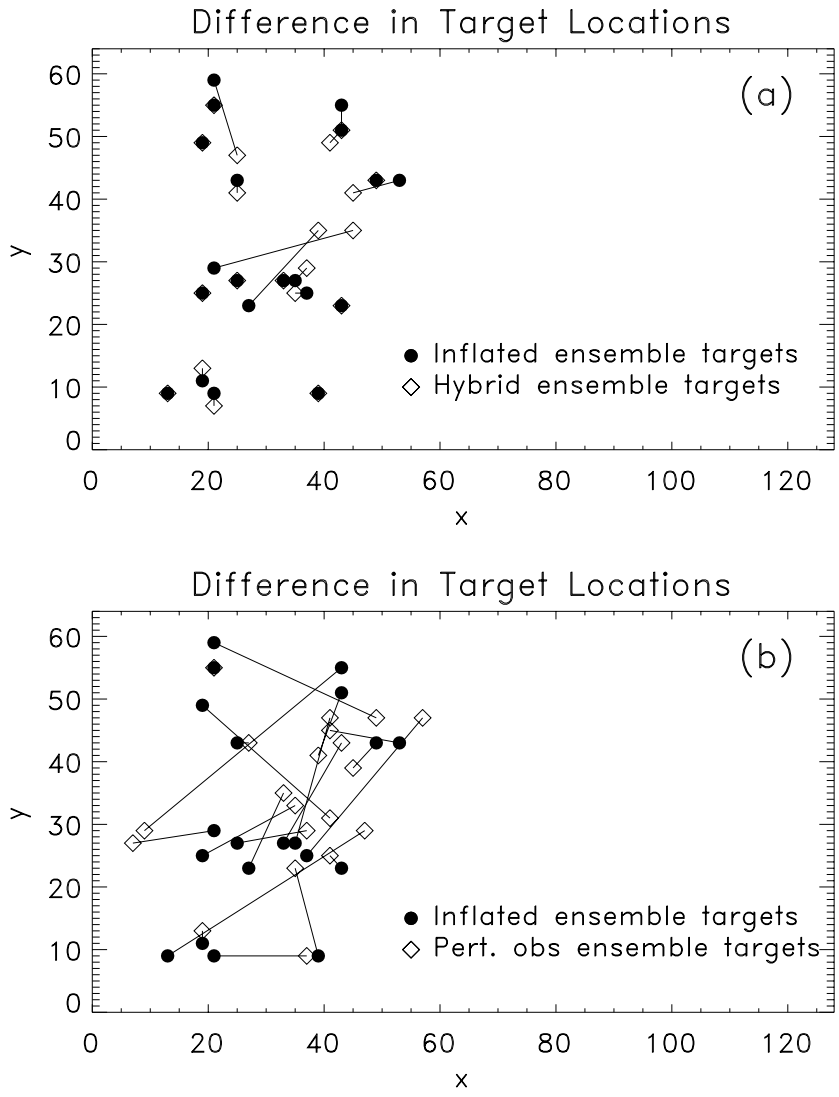

Figure 12. (a) Difference in selected optimal target locations when using inflated ensemble (darkened dots) and hybrid ensemble (diamonds). Darkened diamonds indicate that target locations were identical. Targets for the same case day are connected by solid line. (b) As in (a), but for inflated ensemble vs. perturbed observation ensemble.

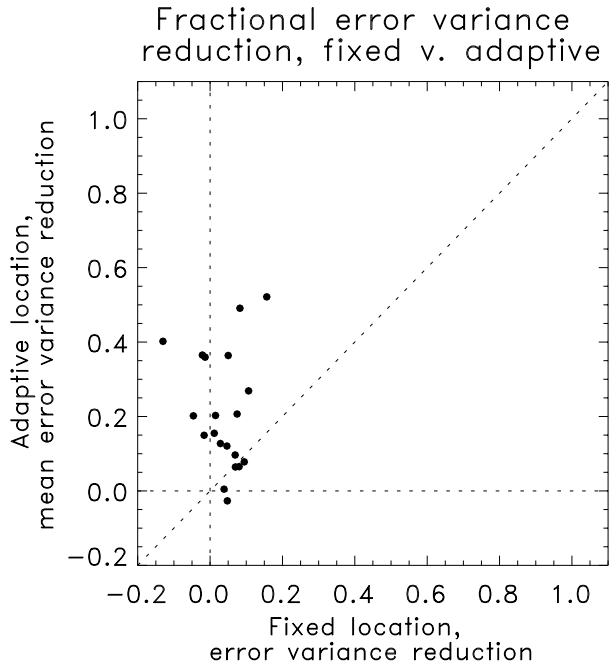

Figure 13. Improvement in ensemble mean analysis error when assimilating targeted vs fixed observations on each of 20 case days.

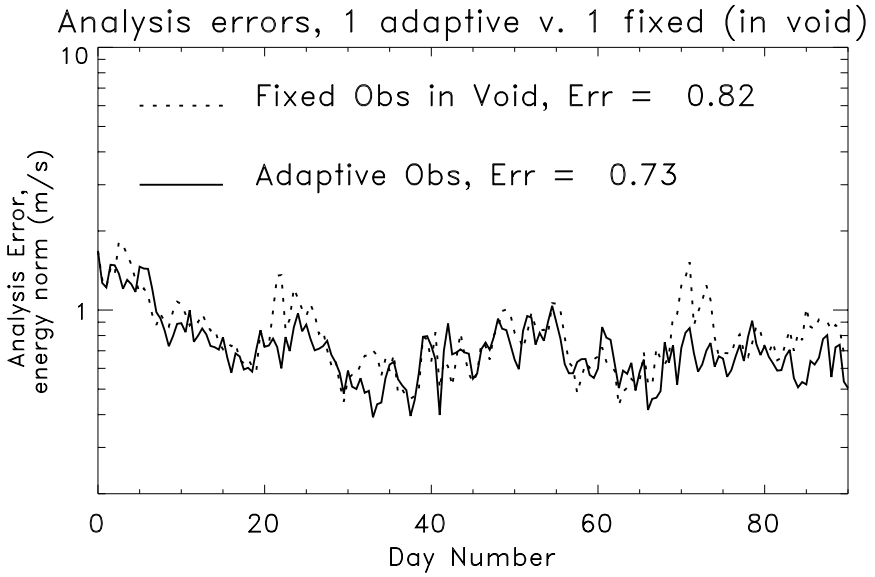

Figure 14. Time series of ensemble mean analysis errors when replacing observation profile at (80,45) in the data assimilation cycle with either a fixed profile at (30,33) or a targeted observation.

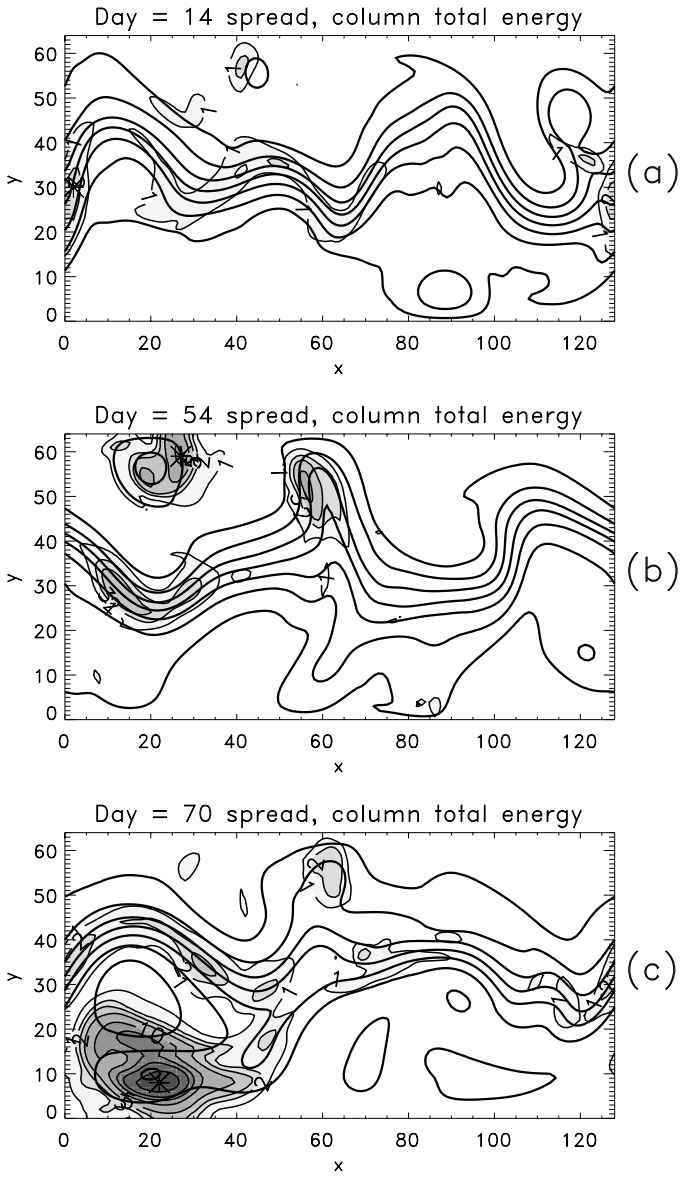

Figure 15. Squared spread in column total energy from the inflated ensemble (shaded) and level 8 geopotential (dark solid lines). Target locations are marked with a star. Contours for spread at 1, 2, 3, 5, 10, 15, 20, 30, 40, 50, and 60 $m^2 s^{-2}$. (a) Case day 14 (compare with Fig. 7b). (b) Case day 54 (compare with Fig. 8b). (c) Case day 70 (compare with Fig. 9b).

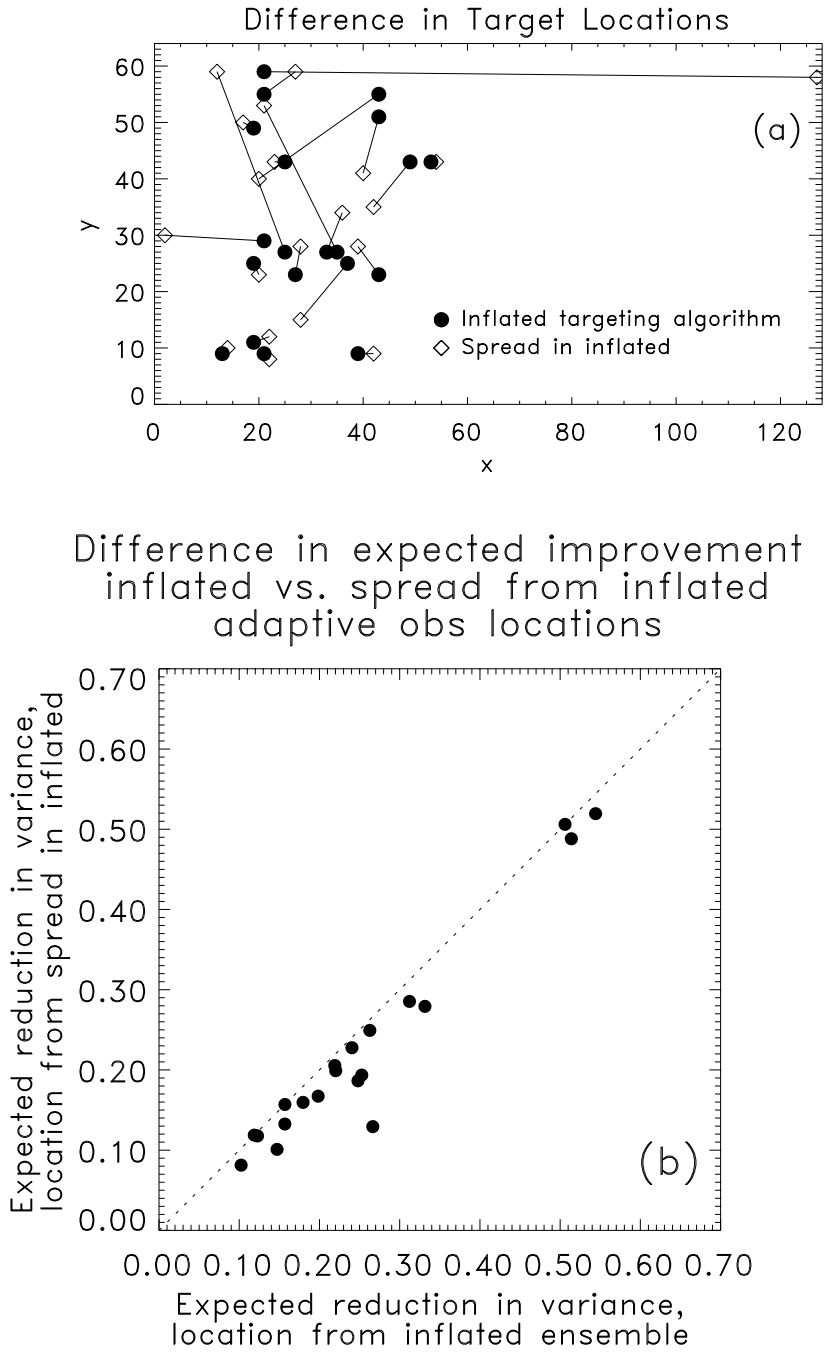

Figure 16. (a) Difference in selected optimal target locations when using full targeting algorithm with inflated ensemble (darkened dots) and targets based on maximum column total energy spread in inflated ensemble (diamonds). (b) Expected reduction in analysis error variance as evaluated from ensemble when targets locations are defined by full algorithm (abscissa) vs. at locations with maximum spread (ordinate).

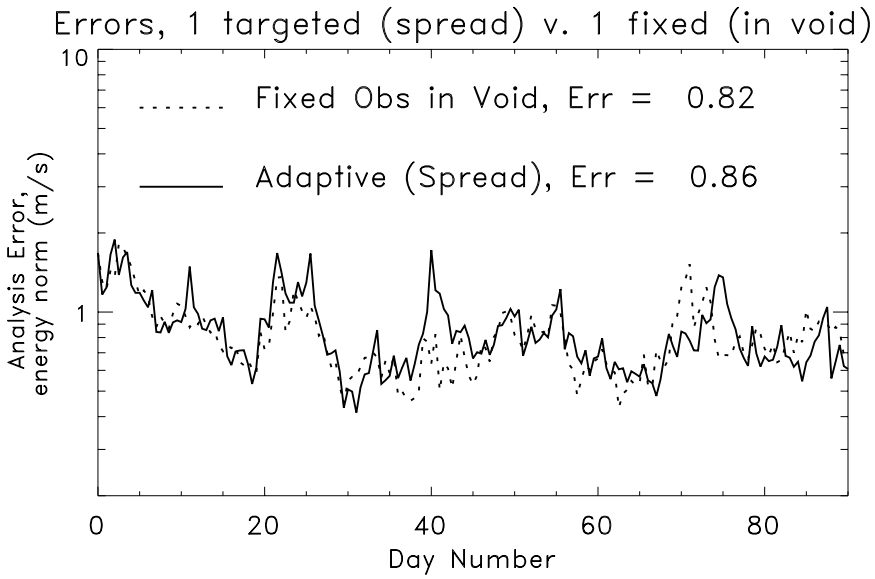

Figure 17. Ensemble mean errors in the energy norm using the inflated ensemble. Solid line indicates errors for where a single sounding from the fixed network at the location x=80,y=45 has been replaced by a sounding at a sounding at x=30, y=33. Dashed line indicates errors where sounding at x=80,y=45 is replaced by a targeted observation with the location determined by the maximum spread.

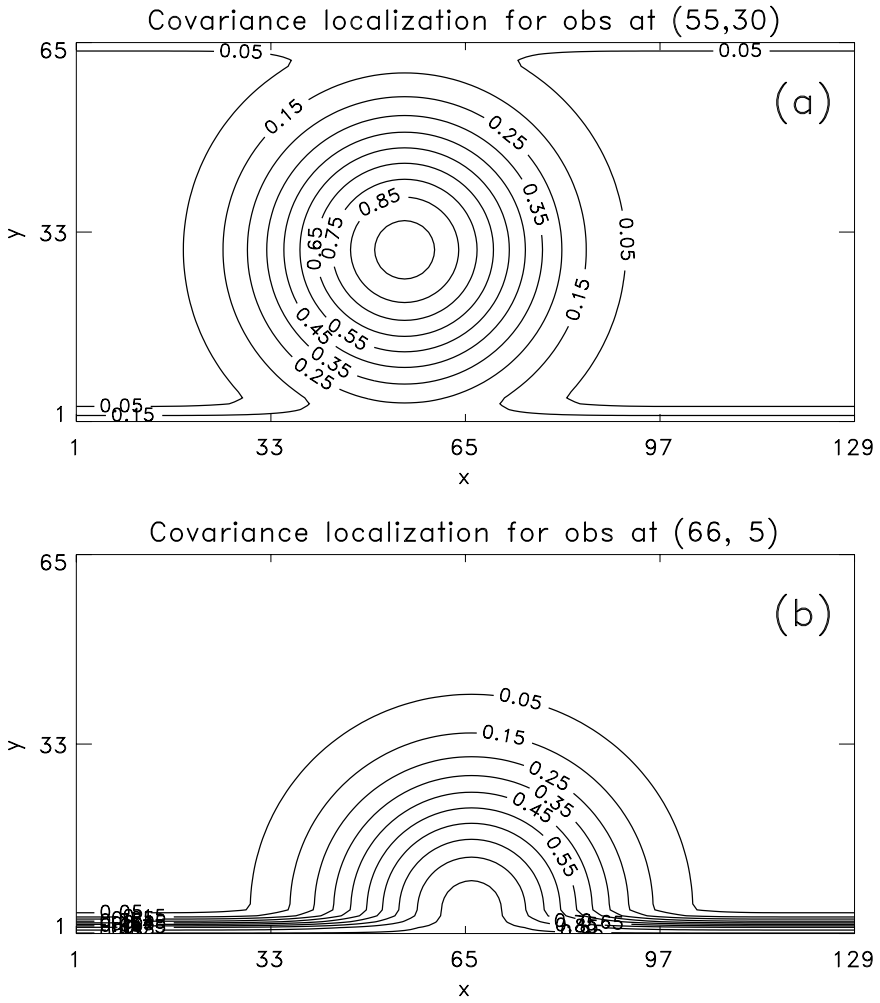

Figure 18. Covariance localization functions for (a) grid point near the center of the channel, and (b) grid point near wall. Correlation length scale in this example is 15 grid points.

Table 1. Observation error variances for temperature (K^2), and u- and v- wind components ($m^2 s^{-2}$).

Level	Pressure (hPa)	T	u	v
1	917	2.82	2.16	1.62
2	771	2.06	3.62	2.71
3	648	1.69	4.96	3.73
4	545	1.69	5.81	4.36
5	458	2.01	6.73	5.05
6	385	2.74	7.71	5.78
7	324	3.59	8.76	6.57
8	272	4.39	8.82	6.61

Table 2. Parameters used for the three data assimilation approaches tested here. α is the percentage weight applied to stationary covariances; c is an inflation factor for the time-mean covariances derived from an EnKF; r is the amount that background forecast deviations about the mean are inflated before the data assimilation proceeds, and l_c is the correlation length scale (in grid points) for the covariance localization.

Experiment	Name	α	c	r	l_c
1	Inflated	0.0	n/a	1.015	28.0
2	Hybrid	0.075	16.0	1.00	25.0
3	Perturbed Obs	1.0	16.0	1.00	n/a